Review: Estimation of Liquid Water Path in Stratiform Precipitation Systems using Radar Measurements during MC3E

By Authors: Jingjing Tian, Xiquan Dong, Baike Xi, Christopher R. Williams, and Peng Wu

General comments:

The authors present a scheme to retrieve rain liquid water path (RLWP) and cloud liquid water path (CLWP) beneath the melting layer in stratiform precipitation. It is known that LWP retrieved from traditional microwave radiometer (MWR) in rainy conditions might be invalid. The authors consider two situations: (1) no cloud detected below the melting layer; (2) cloud is detected below the melting layer. The retrieval of RLWP (namely, situation 1) is based on the method proposed by Williams et al. (2016). In situation (2), to retrieve CLWP they estimate the layer mean rain rate by using the differential velocity technique proposed by Williams et al. (2016), which is expected to be an improvement to the original method (Matrosov. 2009). Using the proposed technique, the authors found that the CLWP is the main contributor to LWP beneath the melting layer when cloud exists.

This is an interesting study that is relevant to the scientific community and is within the scope of AMT. Overall, this manuscript is well written, cites relevant literature and the proposed technique is novel. However, the authors should include a more detailed discussion about the retrieval uncertainty. I recommend it for publication in AMT if the authors take into account the following comments.

We would like to thank this reviewer for his/her time in reviewing this manuscript and providing very clear and insightful suggestions.

Based on this reviewer's suggestion, we made some efforts in the following aspects:

1. **Carefully checked datasets from different observations, which include the ceilometer detected cloud base, the melting base identified from radar observations, for every data point one-by-one.**
2. **Added more uncertainty analyses for retrievals. More details please see the response for the second major comment.**
3. **Checked if there are any relationships between retrievals and the melting base height.**

The reviewer's comments really led us to think deeper of our own study and help us a lot to improve the manuscript through answering the reviewer's questions. This is greatly appreciated. The responses are in bold and black.

We also attached the revised manuscript with track changes at the end of the response to review.

Major comments:

1) Given the generally recognized definition of liquid water path (LWP) is the integral of the liquid water in the whole atmospheric column, I suggest the authors highlight that the LWP in this

manuscript is beneath the melting base in title, abstract and other places where misunderstanding might be induced.

Agree.
The title has been changed to "Estimation of Liquid Water Path *below the Melting Layer* in Stratiform Precipitation Systems using Radar Measurements during MC3E"

Also, clarifications are added in the abstract and other places.
For example, the first sentence of in the abstract changed as "In this study, the liquid water path (LWP) below the melting layer in stratiform precipitation systems is retrieved, which is a combination of rain liquid water path (RLWP) and cloud liquid water path (CLWP). "

2) I believe a more detailed retrieval uncertainty analysis for situation (2) is needed. I would love to see the retrieval uncertainty in Figure 4 and 5 (see examples in Figure 3 f, g, h). In addition, a more thorough comparison with (Matrosov, 2009) regarding the retrieved results as well as the uncertainty would be interesting.

As suggested, we added the retrieval uncertainties in Figure 4 and Figure 5.
Figure 4 shows the retrievals for rain microphysics only. The uncertainties for D_m and rain rate are discussed in our original manuscript (Appendix A). "The uncertainties are estimated using the Monte Carlo method, by first estimating radar measurement uncertainties, constructing a distribution of input radar measurements and then repeating the DVD retrievals for this distribution of input measurements. The details of this "DVD Algorithm" and uncertainty estimation are introduced in Appendix A."

The uncertainties of RLWP (Figure 4c) is estimated based on the uncertainties of RLWC. More specifically, step (1) we estimated the RLWC uncertainties at each height level, which is similar to the uncertainty estimations of D_m and rain rate in Appendix A. Step (2), we calculated the ratios of RLWC uncertainties to mean retrieved RLWC at each height level, which represent percentage values of retrieval uncertainties. Step (3), we calculated the mean ratio of the uncertainties in the whole liquid layer below melting base and regarded this mean ratio as the uncertainties of RLWP.

In the Appendix A we added "The uncertainties of RLWP are estimated based on the uncertainties of RLWC. More specifically, we first estimated the RLWC uncertainties at each height level, and then we calculated the ratios of RLWC uncertainties to mean retrieved RLWC at each height level, which represent percentage values of retrieval uncertainties. Finally, we calculated the mean ratio of the uncertainties in the whole liquid layer below melting base and regarded this mean ratio as the uncertainty of RLWP."

The updated Figure 4 is shown as below:

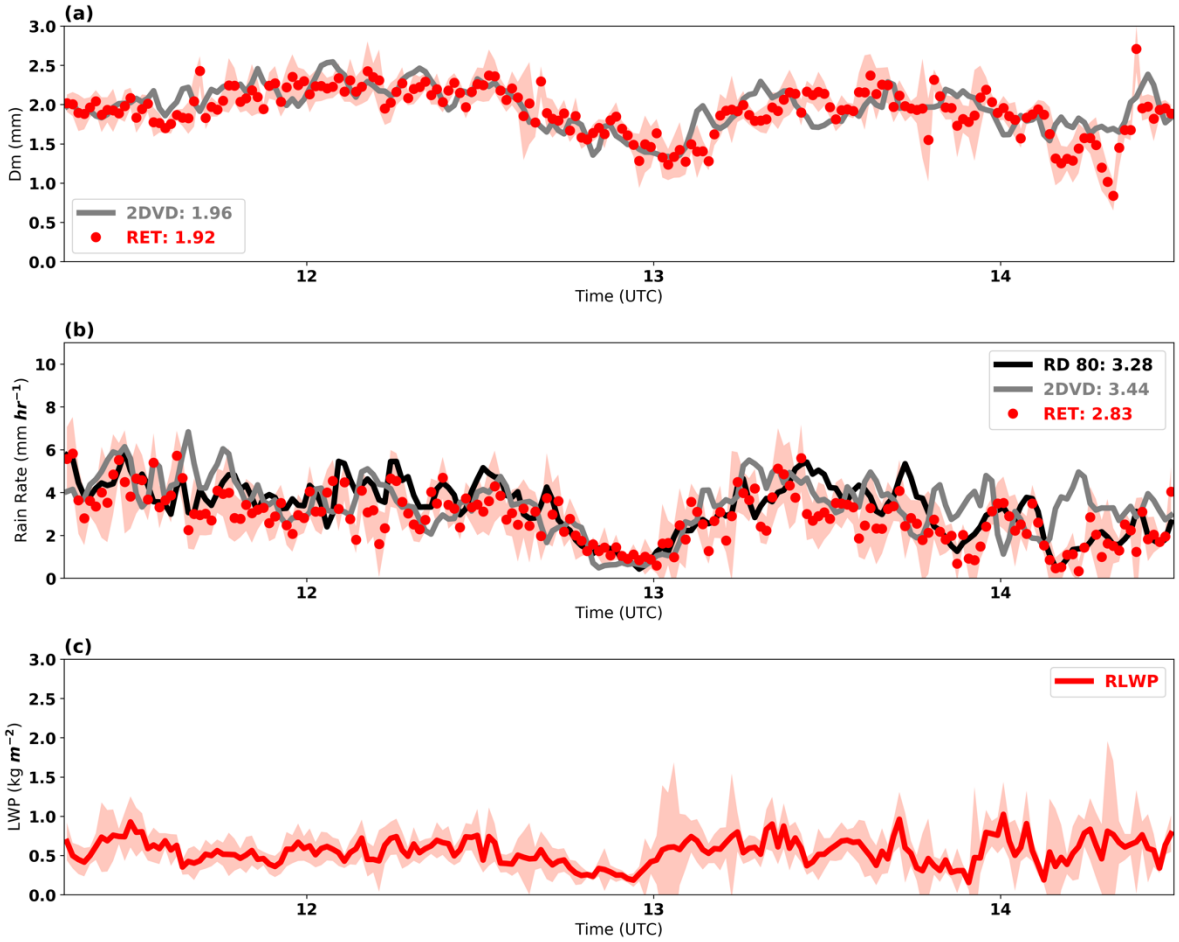

Figure 4. Time series of (a) retrieved (RET) (red dots) and 2DVD surface disdrometer estimated (grey line) D_m, (b) RET (red dots), 2DVD (grey line) and RD-80 (black line) surface disdrometer rain rate estimates, and (c) retrieved rain liquid water path (RLWP, red line) for Case A (May 20, 2011). The red shading areas are the estimated retrieval uncertainties.

In Figure 5, the estimation methods for rain microphysics retrieval uncertainties are the same as those we discussed in Figure 4.

The uncertainty of CLWP is discussed as follows:

CLWP is estimated by, firstly, subtracting the total attenuation (A) from rain attenuation to get the cloud attenuation, and secondly, dividing the cloud attenuation (B) by the cloud water attenuation coefficient.

$$\mathbf{CLWP} = \frac{\mathbf{A} - 2\,\mathbf{C}\,R_{total}}{2\,\mathbf{B}} \quad \mathbf{(1)}$$

The rain attenuation is estimated by the rain attenuation coefficient (C) multiplied by the total rain rate (R_{total}). The attenuation (A) is estimated by comparing the drop in Ka-band reflectivity with the un-attenuated S-band reflectivity. C and B are the coefficients for rain and cloud water attenuation, where C equals ~0.26 dB /km /mm hr^{-1}, and B equals ~0.87 dB / kg m^{-2}. The influence of temperature uncertainties in B on the retrieval errors is minor

compared to the uncertainty of the total attenuation (A) and total rain rate (R_{total}) (Matrosov 2010).

The uncertainty of CLWP is calculated as

$$\Delta CLWP = \sqrt{\left(\frac{\partial CLWP}{\partial A} \times \Delta A\right)^2 + \left(\frac{\partial CLWP}{\partial R_{total}} \times \Delta R_{total}\right)^2} \quad (2)$$

$$\Delta CLWP = \sqrt{\left(\frac{1}{2B} \times A \times Ua\right)^2 + \left(-\frac{C}{B} \times R_{total} \times Ur\right)^2} \quad (3)$$

For given uncertainties of attenuation (Ua) and total rain rate (Ur), the uncertainty of CLWP can be calculated using equation (3). The blue uncertainty bars in Figure 5c show the retrieved CLWP uncertainty with assuming both of the uncertainties of attenuation and total rain rate are 30% (Ua=Ur=30%). It is noted that, due to the variations of the attenuation and total rain rate with time, the estimated uncertainty of CLWP varies point to point.

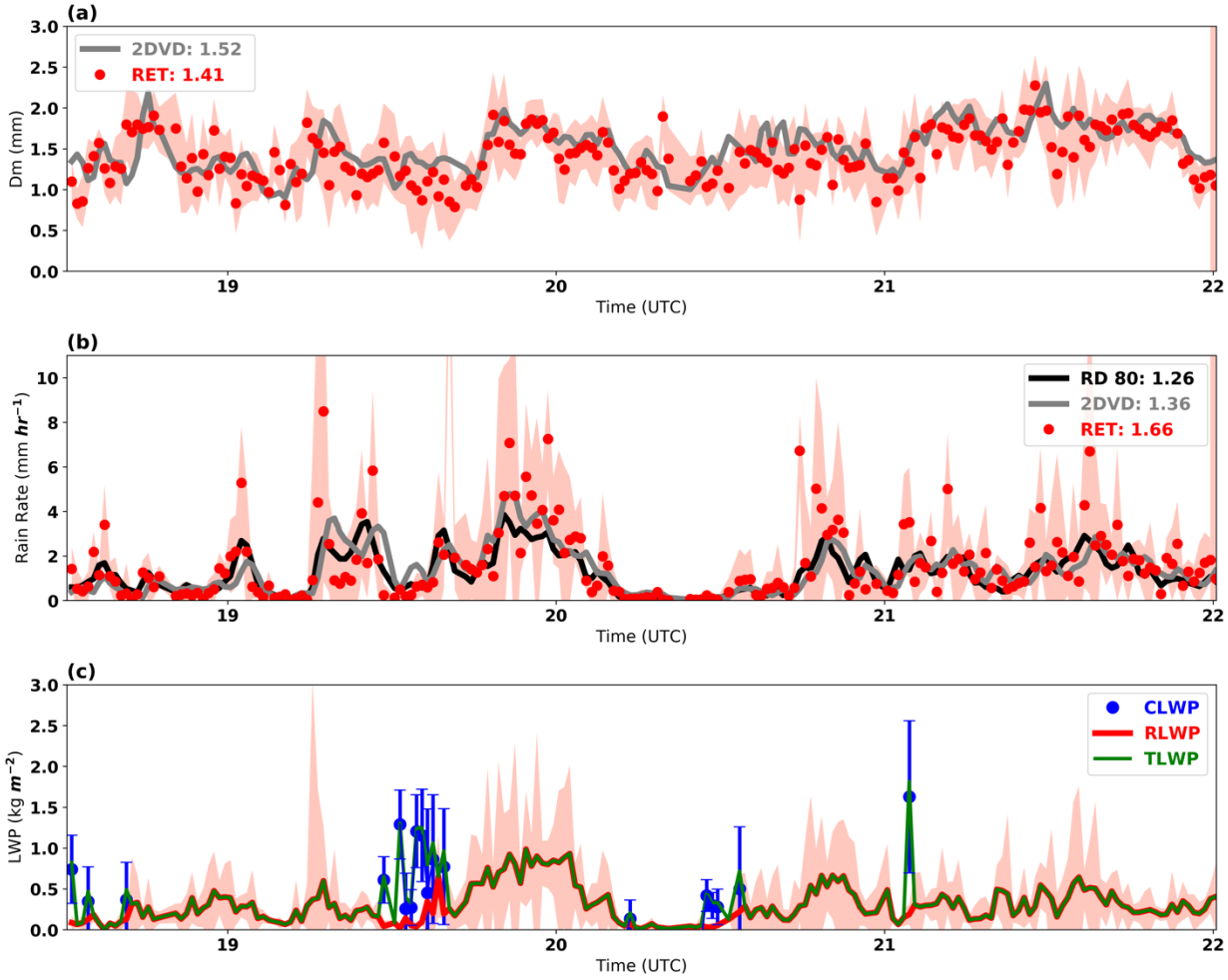

Figure 5. Time series of (a) retrieved (RET) (red dots) and 2DVD surface disdrometer estimated (grey lines) D_m, (b) RET (red dots), 2DVD (grey line) and RD-80 (black line) surface disdrometer rain rate estimates, and (c) rain liquid water path (RLWP, red line),

cloud liquid water path (CLWP, blue dots) and liquid water path (LWP = RLWP+CLWP, green lines) for Case B (May 11, 2011). The red shading area and blue bars are the estimated retrieval uncertainties for rain microphysical properties (D_m, rain rate and RLWP) and CLWP.

In the revision, we added an Appendix B:
"Appendix B: CLWP Uncertainty

CLWP can be estimated as following equation:

$$\mathbf{CLWP} = \frac{\mathbf{A} - 2\,\mathbf{C}\,R_{total}}{2\,\mathbf{B}}. \quad \textbf{(B1)}$$

The rain attenuation is estimated by the rain attenuation coefficient (C) multiplied by the total rain rate (R_{total}). The attenuation (A) is estimated by comparing the drop in Ka-band reflectivity with the un-attenuated S-band reflectivity. C and B are the coefficients of rain and cloud water attenuation with values of ~ 0.26 dB /km /mm hr^{-1} and ~ 0.87 dB / kg m^{-2}, respectively. The influence of temperature uncertainty in B on the retrieval error is minor compared to the uncertainties of the total attenuation (A) and total rain rate (R_{total}) (Matrosov 2010). The uncertainty of CLWP is calculated as

$$\Delta \mathbf{C}LWP = \sqrt{\left(\frac{\partial CLWP}{\partial A} \times \Delta \mathbf{A}\right)^2 + \left(\frac{\partial CLWP}{\partial R_{total}} \times \Delta R_{total}\right)^2} \quad \textbf{(B2)}$$

$$\Delta \mathbf{C}LWP = \sqrt{\left(\frac{1}{2B} \times \mathbf{A} \times \mathbf{Ua}\right)^2 + \left(-\frac{C}{B} \times R_{total} \times \mathbf{Ur}\right)^2} \quad \textbf{(B3)}$$

For given uncertainties of attenuation (Ua) and total rain rate (Ur), the uncertainty of CLWP can be calculated based on equation (B3). "

In Figure 5c, the retrieved CLWP values can be as large as 2~3 kg/m2. It sounds like very large values for me. Since the comparison to MWR LWP is a suspect due to radome wetting, could you compare your retrieved values to observations in non-precipitating warm clouds? It would give an idea of how realistic those values are.

To figure out why we have large CLWP values (e.g., ~2- 3 kg m^{-2}) in the original manuscript, at first, we checked the melting base and cloud base manually and carefully to make sure we use the "best-estimations" of melting base and cloud base in the retrieval.
The new CLWP retrievals are shown in Figure 5c where all CLWP values are smaller than 1.5 kg m^{-2}. Also, as suggested, the retrieval uncertainties are added in the Figure 5. The retrieved CLWP values, especially when taken uncertainties into consideration, are comparable with the estimations of CLWP (Figure 13) in Matrosov (2009). It is clearly seen that the retrieved CLWP values could be larger than 1 kg m^{-2}. After the revision, the mean and median values of the retrieved CLWP are 0.56 and 0.45 kg m^{-2} for all cases (Figure 6).

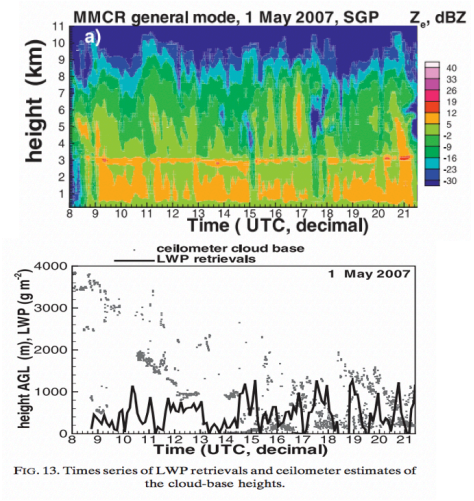

FIG. 13. Times series of LWP retrievals and ceilometer estimates of the cloud-base heights.

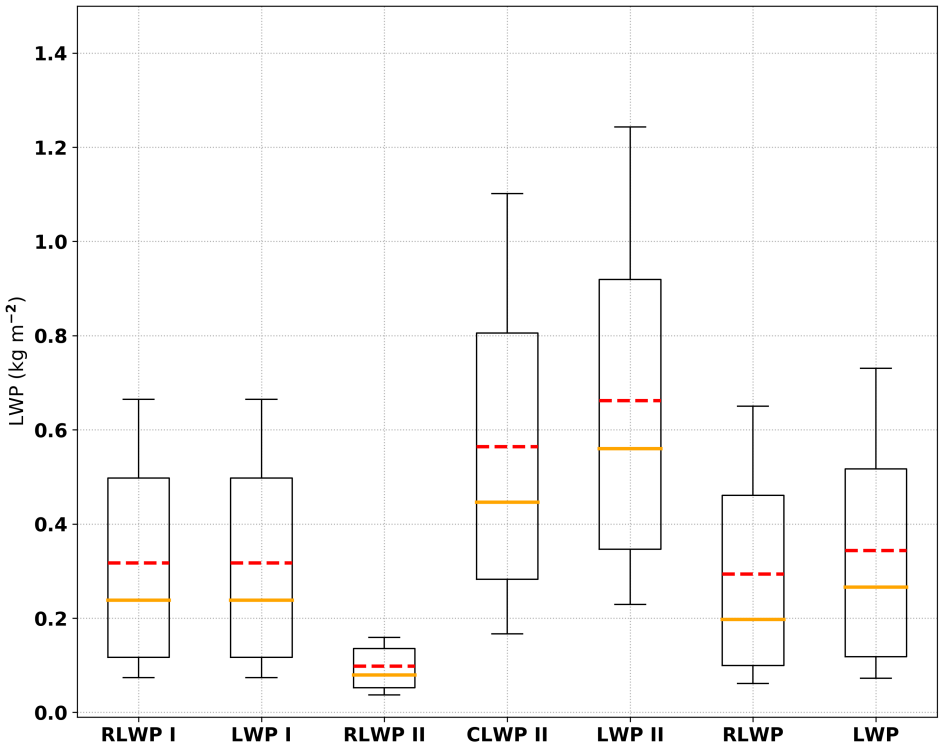

Figure 6. Box and whisker plots of retrieved RLWP, CLWP and LWP for situation (I), (II) and all samples. The horizontal orange line within the box indicates the median, boundaries of the box represent the 25th- and 75th -percentile, and the whiskers indicate the 10th- and 90th -percentile values of the results. The red dash lines represent the mean values.

Since the comparison to MWR LWP is a suspect due to radome wetting, could you compare your retrieved values to observations in non-precipitating warm clouds? It would give an idea of how realistic those values are.

The algorithms in this study do not work for the non-precipitation warm clouds, as there is almost no observations/reflectivities at 3 GHz radar for low-level warm cloud. Thus, we did not compare our retrieved CLWP with MWR-retrieved CLWP directly.
But, to get a better idea of how realistic of retrieved CLWP values, as suggested, we checked the CLWP from MWR for non-precipitating warm clouds. An example of CLWP from MWR on May 13, 2011 is shown as below. Observations (Ka-band cloud radar and MWR-LWP) are from ARM SGP site. We found the CLWPs are less than 0.4 kg m^{-2} in general.

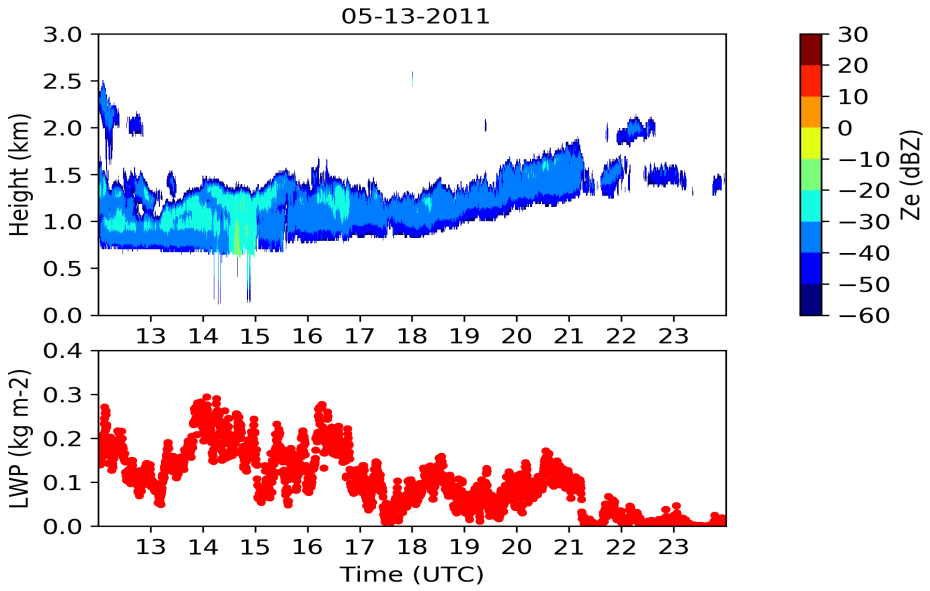

3) Figure 1. Have you checked that how often the ceilometer signal is totally attenuated?

Yes, we checked the ceilometer signal attenuation rate, which is 11.7 %.

The black dots in Figure 1 seem indistinguishable from the melting layer for me. I suggest the authors to use a separate time series plot to show the heights of melting top/base and cloud base, which may help readers to understand the difference between situation 1 and 2 better.

Thanks for the suggestion of adding a subplot to show the melting and cloud base to make it clearer to readers. Updated Figure 1 is shown as below.

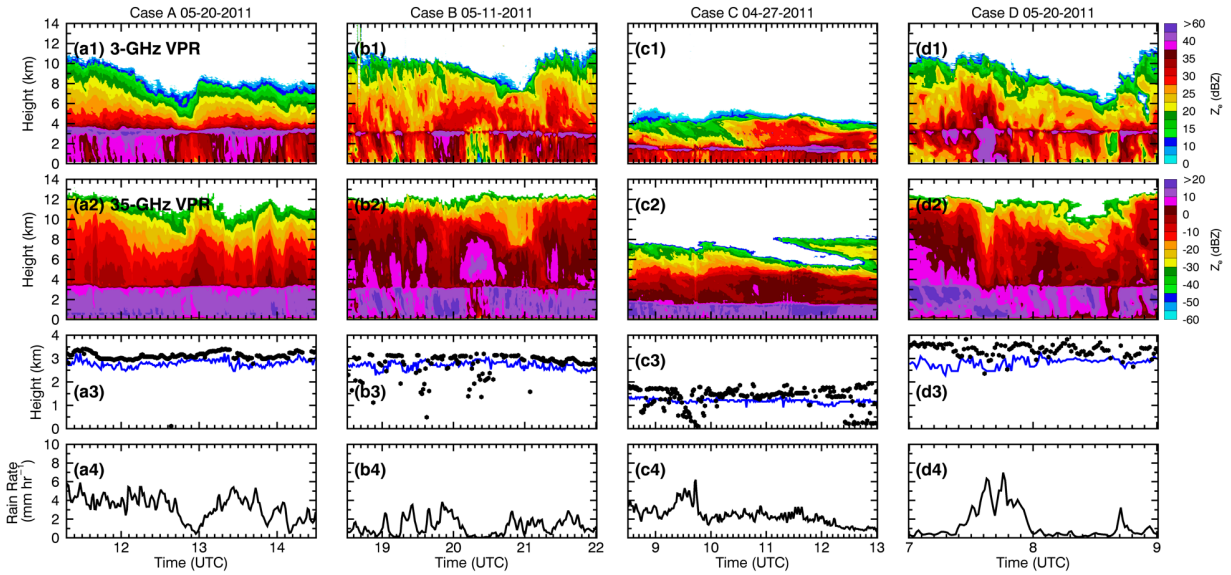

Figure 1. Time series of (a1) radar reflectivity (Z_e) from NOAA 3-GHz vertical pointing radar (VPR), (b1) radar reflectivity from ARM 35-GHz VPR, (c1) melting base (blue lines) and cloud base (black dots), and (d1) rain rates from RD-80 surface disdrometer measurement for Case A (20 May 2011, 11:20 – 14 :30 UTC); (b1)-(b4) for Case B (11 May 201, 18:30 – 22 :00 UTC); (c1)-(c4) for Case C (27 April 2011, 8:30 – 13 :00 UTC); (d1)-(d4) for Case D (20 May 2011, 7:00 – 9 :00 UTC). Note that the ranges of radar dBZ values are different in 3-GHz and 35-GHz radars.

4) Both RLWP and CLWP are dependent on the geometrical thickness of rain and cloud layers, have you considered the changes of the melting layer height? If there are significant changes of melting layer height, RLWP will be affected.

To better answer this question, we generate the following figure.

In the upper panel, the x-axis is the melting base height (the height we integrate RLWC), and the y-axis is the RLWP. The data are separated for each case using different colors. Case C (in cyan color) has lower melting base heights and smaller RLWP compared to other cases. We agree that, in general, the retrieved RLWP increases with the increased melting base. However, there are some exceptions. For example, some RLWP values for Case D are much lower (< 0.25 kg m-2) at higher melting bases (2.5-3 km), which warrants a further study.

In addition to investigate the RLWP, we also checked the mean RLWC for each case (lower panel). Even though the RLWP differences are large between case C and other cases, the RLWC differences are not that significant compared to the RLWP differences.

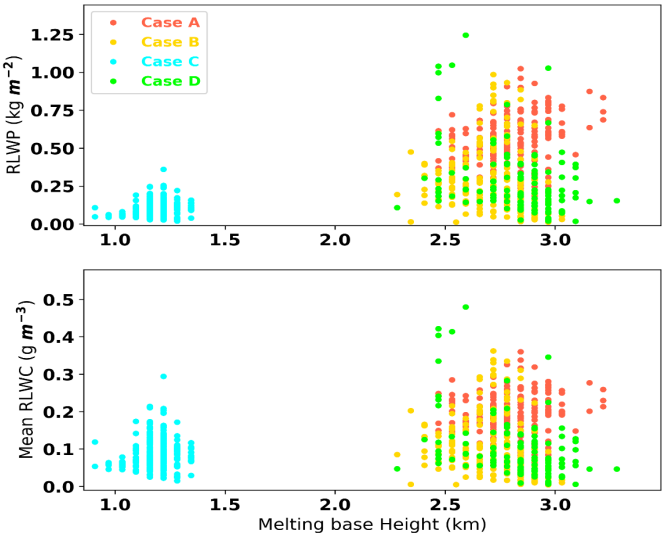

5) Figure 7. The retrieved LWP in Figure 7b seems to be weakly linked to rain rate, though high correlation between the rain rate and RLWP is shown in Figure 4 and 5. Can you explain this?

Based on another comment/suggestion given by this reviewer, "Have you considered using a scatter plot to show the relations between RET and MWR with rain rate indicated by color?", we generated a figure as below.

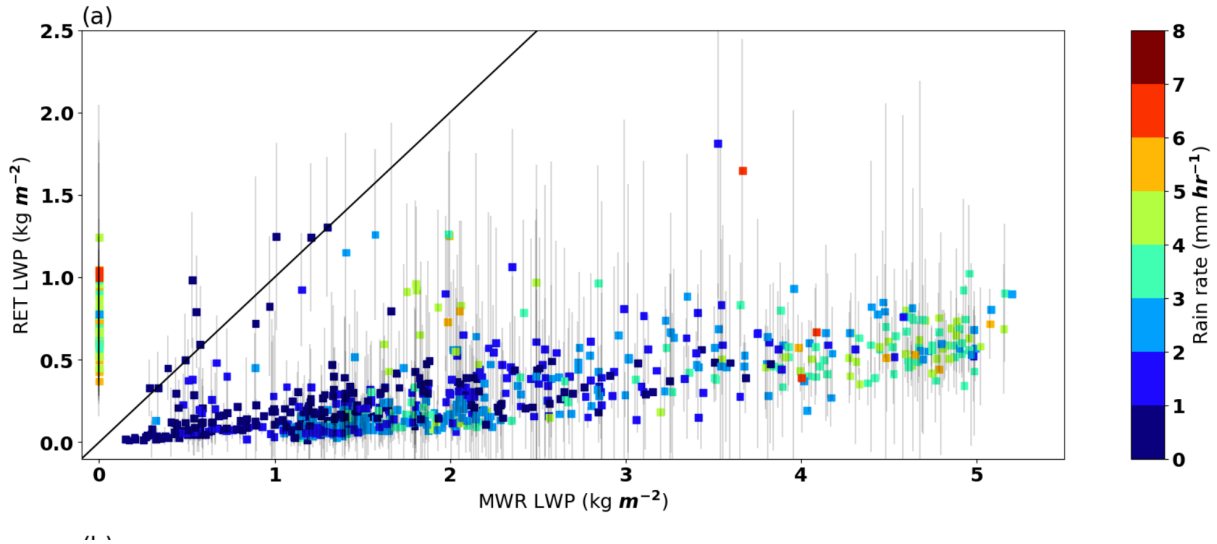

This figure shows the comparisons between LWPs retrieved from microwave radiometer measured brightness temperatures (MWR, in x-axis) and LWPs retrieved from this study (RET, in y-axis, with estimated uncertainty in gray lines). The rain rates are indicated by colors. The black line is 1:1 line.
In the revised plot, we do find that the retrieved LWPs are slightly correlating rate rates, but not as strong as the MWR-retrieved LWPs.

In the revision: "The corresponding LWP uncertainties are also provided as the grey error bar for each retrieval with rain rate indicated by colors. The MWR-retrieved LWPs increase with increased rain rate, and much larger than the new LWP retrievals at high rate rates. The newly retrieved LWPs weakly correlate with rain rates, and most values are less than 1.0 kg m^{-2}, especially at high rain rates."

Have you tried to quantify by how much the MWR overestimates the LWP for cases with the similar melting base height?

Yes, we were trying to find if the "overestimations" from MWR is highly related to the melting base height, but unfortunately, we think it is hard to quantify or give a general relationship, based on these scattered points as shown below.

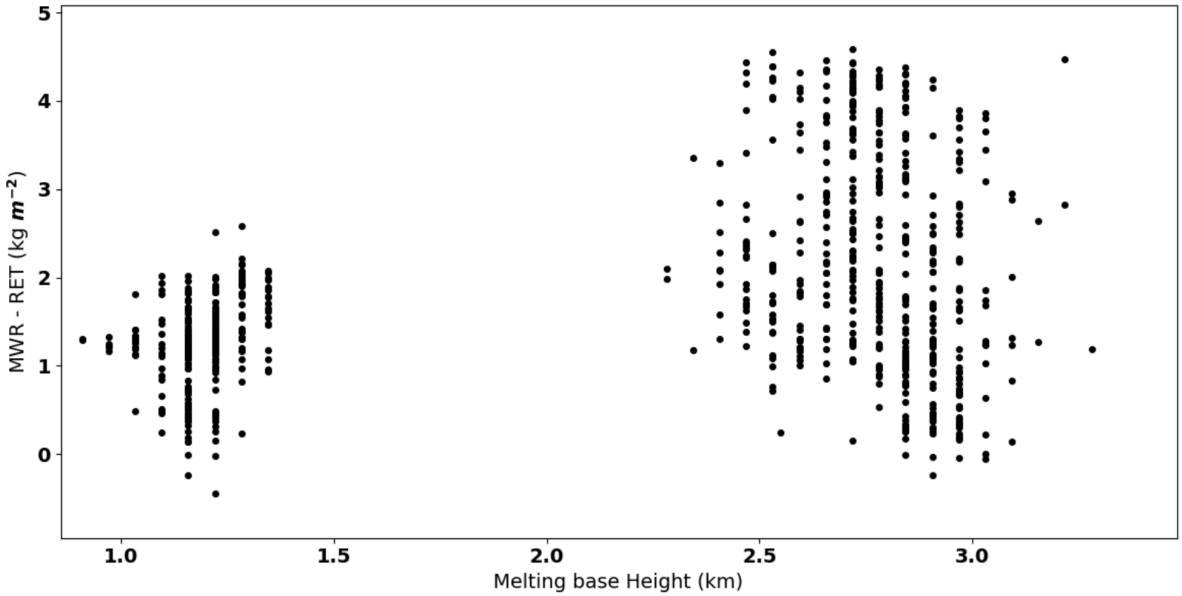

6) The authors compare their finding to the study of Lebsock et al. (2011). However, they study warm clouds while the presented research focuses on cold cloud precipitation. To what extent this comparison is meaningful?

The ratio of CLWP/RLWP comparison between cold and warm cloud may be confusing. They are different type of clouds. We deleted the comparisons in the revision.

Minor issues:

- Please check the references (e.g., line 582, should be 'J. Appl. Meteor. Climatol.'), and follow AMT's requirement on literature format.

Yes, references are written in AMT format in the revision.

"Matrosov, S. Y.: A method to estimate vertically integrated amounts of cloud ice and liquid and mean rain rate in stratiform precipitation from radar and auxiliary data, J. Appl. Meteor. Climatol., 48, 1398–1410, doi:10.1175/2009JAMC2196.1, 2009"

- Figure 3 d. It seems to me that the negative differential velocity in the melting layer is a bit large. Have you checked the matching of the ranges between those two radars?

Yes, we checked the radar data matching both temporally and vertically. The negative differential velocity is not as large as -0.8 m/s always. Several examples are given in the figure below.

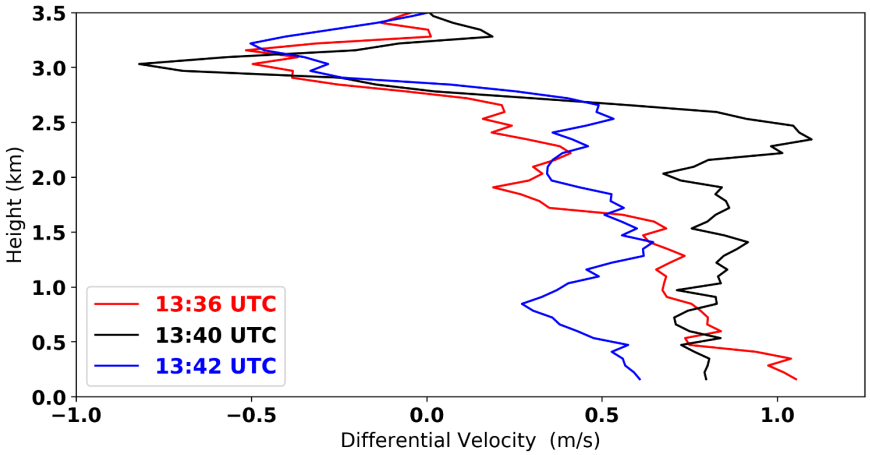

- Figure 4 and 5. Use standard format for time, such as 12:30 instead of 12.5.

Yes, modified.

- Figure 4b and 5b. It seems that the retrieved rain rate agrees better with more stable precipitation (e.g., 12.7 - 13.1 in Figure 4b). But what are the reasons for those obviously overestimated retrievals in Figure 5b?

As suggested by the reviewer, we added the retrieval uncertainties in Figure 4 and Figure 5. Even though the retrievals (red points) are sometimes much larger than the surface observations (grey or black lines) in Figure 5b, we found the observations are within the retrieval uncertainties (shaded area) generally.

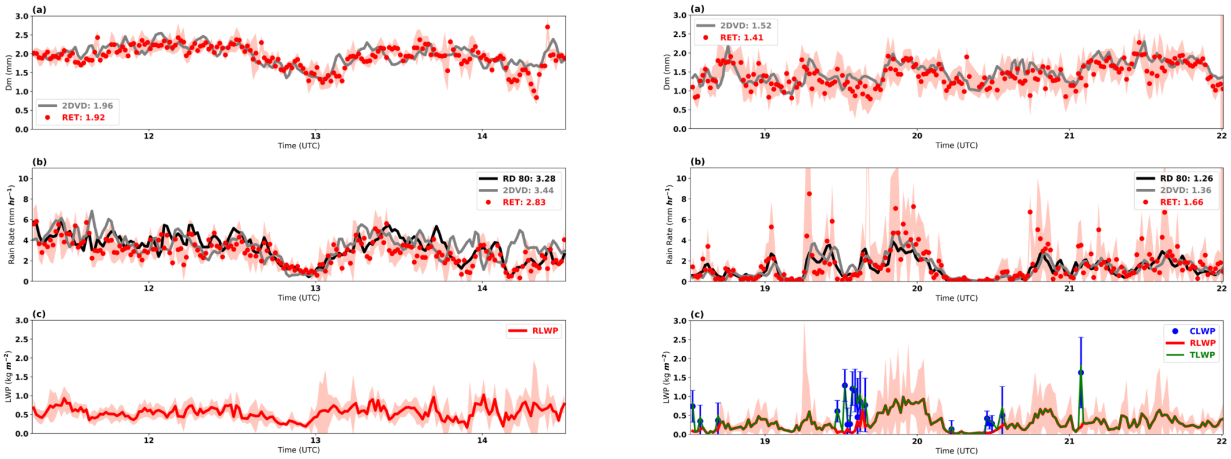

We would also like to address this question on the basis of retrieval mathematically.

In the retrieval, a normal distribution is generated first for each 1-min/60-m resolution radar measurements using their corresponding mean and standard deviations. For example, the temporal resolution for 3-GHz VPR is seven seconds, thus there are about nine radar reflectivities observed for one minute. A normal distribution is generated using the mean and standard deviations of these nine observed radar reflectivities.

Similarly, we generated the normal distributions for Doppler velocity difference and Ka-band spectrum width.

After generating the normal distributions, we randomly select 100 groups of members from those (DVD, SV_{35GHz}, Z_{3GHZ}) normal distributions to form 100 realizations, and then produce 100 separate output estimates. *The final retrieval is the mean of the 100 solutions*, and the retrieval uncertainty is the standard deviation of the 100 solutions.

For the stable precipitation, the standard deviations of inputs are much smaller than those in the unstable precipitation. Thus, the stand deviations of retrievals would be larger in the unstable precipitation, and the differences between observations and mean values of retrievals could be large.

- Figure 7. It seems to me that the use of error bar is a bit puzzling, since for a rain rate bin the retrieved/measured LWP are under different conditions (e.g., different melting base). Have you considered using a scatter plot to show the relations between RET and MWR with rain rate indicated by color?

Figure 7 is changed following the suggestion. This plot is also discussed in the response to reviewer for the former question.

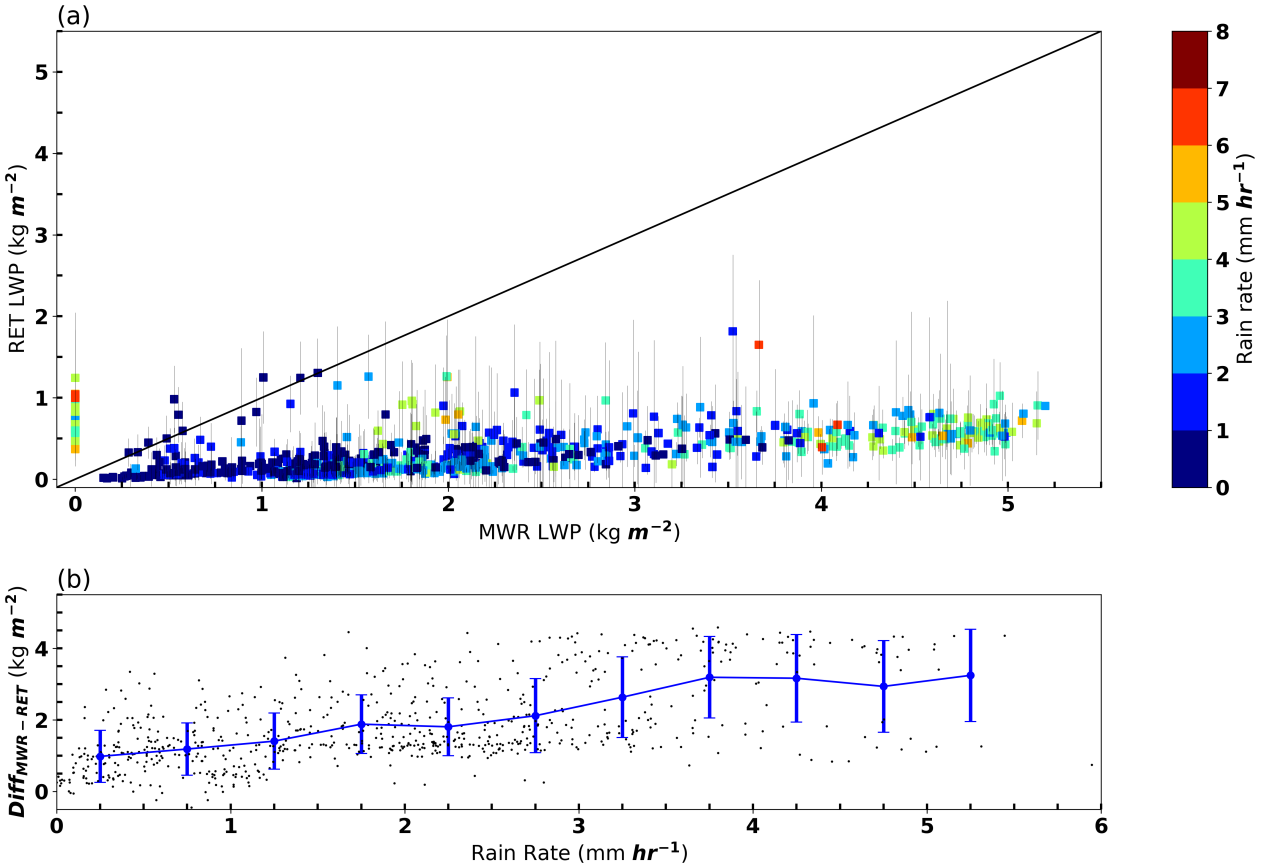

Figure 7. (a) Comparisons between LWP from microwave radiometer (MWR, in x-axis) and LWP retrievals from this study (RET, in y-axis, with estimated uncertainty in black bars) with color-coated rain rate values. (b) the LWP differences between two estimations (MWR-RET), shown as a function of rain rate.

- Line 39, 'with-cloud'

Yes, modified.

- Line 49, 'is still'

Yes, modified.

- Line 62, 'they are known'

Yes, modified.

- Line 109, '. However,'

Yes, modified.

- Line 136, 'bright band'

Yes, modified.

- Line 179, 'with the aid of'

Yes, modified.

- Line 229, 'limiting'

Yes, modified.

- Line 235, 'B'

Yes, modified.

- Line 292, 'relatively'

Yes, modified.

- Line 339, 'samples'

Yes, modified.

- Line 347-358, RLWP/CLWP > 2 in Lebsock et al. (2011) while in this study RLWP/CLWP is on average much smaller, how to explain such difference?

The ratio of CLWP/RLWP comparison between cold and warm cloud may be confusing. They are different type of clouds. We deleted the comparisons in the revision.

- Line 348, 'having not'

Yes, modified.

- Line 359, 'compared them'

Yes, modified.

- Line 363, 'possibly due to'

Yes, modified.

- Line 424, delete either of the 'separately'

Yes, modified.

The paper describes a technique for estimating the LWP in stratiform precipitation. The methodology is applied to 20 case studies collected during MC3E. The paper is generally clear and well written and targets a very important issue, the partitioning between cloud and rain liquid contents in precipitating clouds (though it finds only a partial solution to it).

We appreciate the reviewer for his/her time and effort for reviewing this paper. Especially, the second comment really helps the first author to gain some experiences in radiative transfer calculation and get a deeper understanding on the cloud water path retrievals at (unpolarized/polarized) microwave radiometer channels. We thank him/her for the constructive comments and suggestions. The responses are in bold and black.
We also attached the revised manuscript with track changes at the end of the response to review.

Some comments 1) It must be clear from the beginning that the methodology is only capable of computing the LWP below the bright band and that the methodology is not applicable in presence of liquid above the melting layer.

Agree. The title has been changed to "Estimation of Liquid Water Path *below the Melting Layer* in Stratiform Precipitation Systems using Radar Measurements during MC3E"
Also, clarifications are added in abstract and other places.
For example, the first sentence of in the abstract changed as "In this study, the liquid water path (LWP) below the melting layer in stratiform precipitation systems is retrieved, which is a combination of rain liquid water path (RLWP) and cloud liquid water path (CLWP). "

2) The explanation on the overestimates of LWPs by radiometers is pretty convoluted (at the moment it is a full page, page 17) and needs to be simplified.

To better understand this bit in first place you could compute the extinction (and scattering) coefficients like in Fig.10 of your second reference. Clearly raindrops are much more efficient in extinguishing radiation than cloud droplets (but this depends on the size of the raindrops! so I do not agree with the 2/3 statement at line 382). Yes I agree the single scattering albedo also is much larger.

Second you could use RT computations (e.g. Eddington or a successive order approximations where you can simplify all equations because for your purpose you can neglect polarization effects and you can assume spherical particles only) to compute the TBs for the two channels used by the radiometers to show the enhancement when r-LWP instead of c-LWP is present. Fig4 of your second reference shows an example of that for 30 degrees elevation angle (here you need to repeat the computation at nadir and for the frequencies of the radiometer). But from that figure it is clear the enhancement in case of rain: compare the TBs e.g. for c-LWP=1 kg/m^2 vs r-LWP=1 kg/m^2.

Following the suggestions, we first generated Figure B as the Figure 10a in Battaglia et al. (2009). We calculated the extinction cross section per volume as a function of the drop equivolume diameter for the two frequencies/channels in MWR (23.8 GHz and 31.4 GHZ) with a T-matrix method. It is notice that the extinction cross section increases with increased diameter when the diameters are smaller than 3 mm. This indicates the extinction (cross

section) for rain drops (diameter > ~ 50 um) is much larger than that for cloud droplets (diameter < ~50 um).

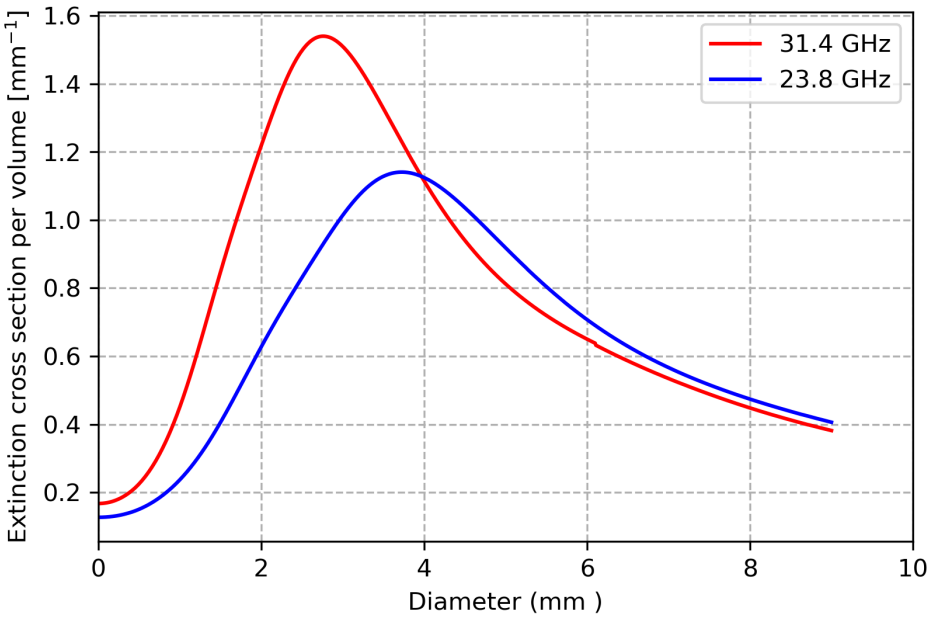

Figure B. The extinction cross section per volume as a function of the drop equivolume diameter for the two frequencies in MWR (23.8 GHz and 31.4 GHZ).

Secondly, we also generated Figure C as the Figure 10 b in Battaglia et al. (2009). We calculated the extinction coefficient as a function of RLWC for populations with three different drop size distributions (DSDs). The DSDs are modeled according to the exponential Marshall and Palmer (MP) distribution $N(D) = N_0 e^{-\Lambda D}$. N_0=8000 m^{-3} mm^{-1}. N_0 is changed to 4000 and 32000 m^{-3} mm^{-1} to represent thunderstorm and drizzle DSDs. More details of the DSDs please see Battaglia et al. (2009).

Figure C clearly shows the extinctions of cloud and rain also are DSD-dependent. For example, at 31.4 GHz, even though the RLWC is the same, the extinctions are much larger from the precipitation with the thunderstorms and MP DSDs than the extinctions from light precipitation with the drizzle DSD.

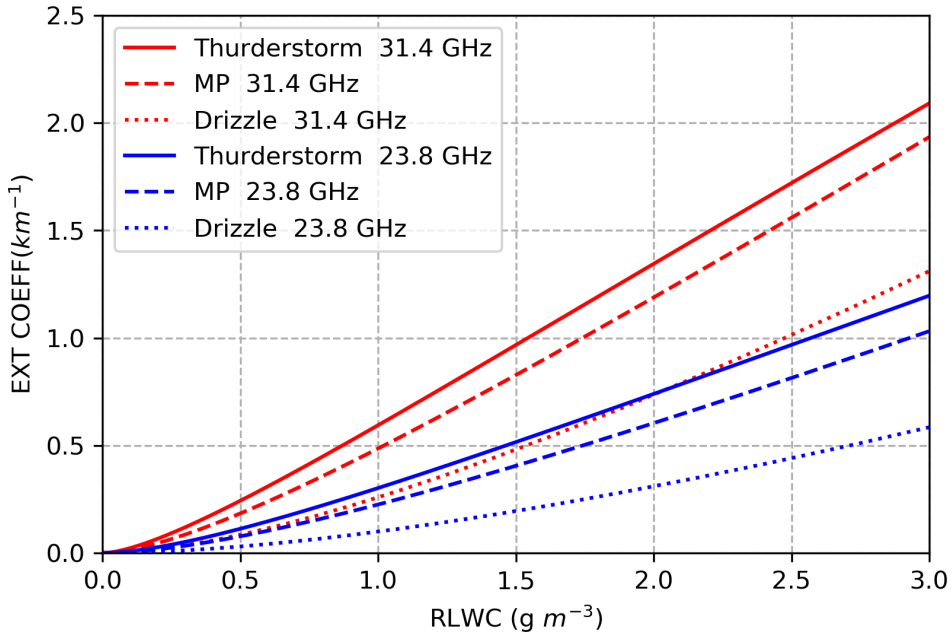

Figure C. The extinction coefficient as a function of RLWC for precipitations with three different drop size distributions (DSDs) in which they represent heavy precipitation (thunderstorm), moderate precipitation (M&P) and drizzle precipitation (drizzle).

Furthermore, we follow the suggestion to calculate the brightness temperatures at 23.8 and 31.4 GHz channels using the MicroWave Radiative Transfer (MWRT) model. Five different sensitivity tests are generated with five combinations of CLWP and RLWP values (Table A). Table A lists the results and clearly demonstrates that the brightness temperatures in channels increase with increased cloud water amount (larger CLWP) and the rain water amount (larger RLWP). Comparing the results from test #2 and #3, it is clearly seen that the brightness temperatures contributed by rain are 31 and 51 K more than that contributed by cloud at the frequencies of 23.8 and 31.4 GHz, even though their LWPs are the same (1 kg m^{-2}) in these two tests.

Table A. The brightness temperatures (TB) at 23.8 and 31.4 GHz for different assumptions of CLWP and RLWP

Sensitivity Test	CLWP (kg m^{-2})	RLWP (kg m^{-2})	TB at 23.8 GHz	TB at 31.4 GHz
#1	2	0	197.20	196.28
#2	1	0	186.34	177.49
#3	0	1	217.28	228.20
#4	0	2	254.51	272.09
#5	1	1	225.37	239.88

The figures and table listed above have been added in the Appendix B in the revision. As suggested, the explanation of overestimation of LWP from microwave radiometer is simplified in the revision. "The increase of MWR-retrieved LWP during raining periods is possibly due to the "wet radome" effect, where the deposition of raindrops on the instrument's radome can cause a large increase in the measured brightness temperatures (Cadeddu et al., 2017). In addition to the issue from standing water on the radome, the extinctions due to raindrops also affect MWR retrievals. The extinction for rain is much larger than that for cloud (Sheppard, 1996), and thus, the small amount of rain water could enhance the measured brightness temperature significantly. More details of extinctions and brightness temperature calculations at MWR channels are shown in Appendix C. "

"Appendix C: Calculations of Extinction and Brightness Temperature at Microwave Radiometer Channels

To better explain the "overestimation" issue of MWR-retrieved LWP during raining periods, several examples are given in this appendix. We first calculated the extinction cross section per volume as a function of the drop equivolume diameter for the two frequencies in MWR (23.8 GHz and 31.4 GHZ) with a T-matrix method (Figure B). It is clearly shown that the extinction cross section increases with increased diameter when the diameters are smaller than 3 mm. This result reveals that the extinction (cross section) for rain drops (diameter > ~50 um) is much larger than that for cloud droplets (diameter < ~50 um). We also calculated the extinction coefficient as a function of RLWC for populations with three different drop size distributions (DSDs). The DSDs are modeled according to the exponential Marshall and Palmer (MP) distribution $N(D) = N_0 e^{-\Lambda D}$, where N_0=8000 m^{-3} mm^{-1}. N_0 is changed to 4000 and 32000 m^{-3} mm^{-1} to represent thunderstorm and drizzle DSDs. More details of the DSDs please see Battaglia et al. (2009). Figure C clearly shows the extinctions of cloud and rain also is DSD-dependent. For example, at 31.4 GHz, even though the RLWC is the same, the extinctions are much larger from the precipitation with the thunderstorms and MP DSDs than the extinctions from light precipitation with the drizzle DSD.

In addition, the brightness temperatures at 23.8 and 31.4 GHz channels are calculated using the MicroWave Radiative Transfer (MWRT) model. Five different sensitivity tests are generated with five combinations of CLWP and RLWP values (Table A). Table A lists the results and clearly demonstrates that the brightness temperatures in channels increase with increased cloud water amount (larger CLWP) and the rain water amount (larger RLWP). Comparing the results from test #2 and #3, it is clearly seen that the brightness temperatures contributed by rain drops are 31 and 51 K more than that contributed by cloud droplets at the frequencies of 23.8 and 31.4 GHz, even though their LWPs are the same (1 kg m^{-2}) in these two tests.

3)Also a key effect in enhancing brightness temperature is the presence of the melting layer (relevant literature must be cited).

Yes, Battaglia et al (2003) found the brightness temperature generally increases if mixed-phase precipitation is included.

In the revision, "The LWP differences between MWR retrieval and this study could be caused by the following reasons. 1) MWR-retrieved LWP represents the entire vertical

column (RWLP and CLWP below melting layer, large water coated ice particles in the melting layer and supercooled LWCs above the melting layer), while our retrieval only represents the LWP below the melting base. As Battaglia et al (2003) pointed out the brightness temperature generally increases if mixed-phase precipitation is included. 2) The MWR radome was wet during the raining periods and the deposition of raindrops on the radome can cause a large increase in the measured brightness temperatures (Cadeddu et al., 2017). 3) Large extinctions due to rain drops would affect MWR retrievals. 4) Uncertainties exist in the retrieved LWP from this study."

4)I found also the discussion at line 315-324 a bit confused: I am not sure why you want to include other disdrometers located within 5 km. I would suggest to delete it.

As suggested, we only include the comparison from the closed 2DVD and RD-80 with retrievals. The comparisons between measurements from other 2DVDs and the corresponding discussions are deleted.

5) Figure A: it would be good to see also contour lines with the values of mu.

As suggested, the contour lines with the miu values are added in the Figure A (b).

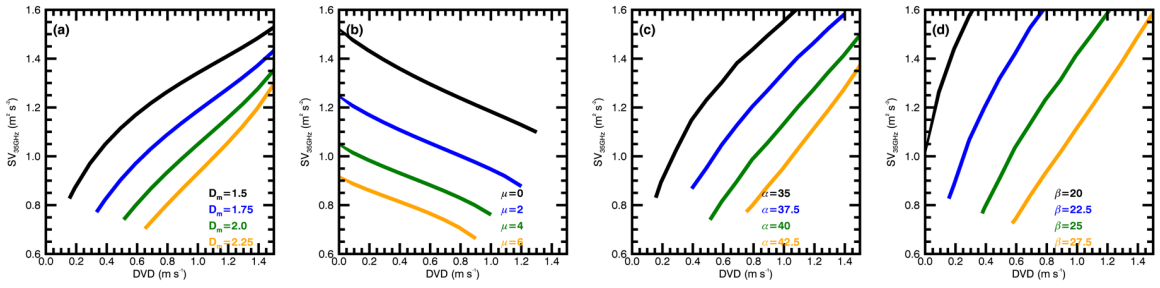

Figure A. Comparisons of (a) mass-weighted mean diameter D_m (mm), (b) shape parameter μ, (c) parameter α= 10 log(Z_{3GHz}/RLWC), and (d) parameter β = 10 log(Z_{3GHz}/RR) calculated as functions of Doppler velocity difference (DVD) and spectrum variance at 35 GHz (SV_{35GHz}). Note that the units of RLWC and RR are g m^{-3} and mm hr^{-1}.

6) Several typos (e.g. line 196, 292)

Thanks for the carefully check. The typos are corrected.

7) The names of the parameters in the Appendix are not optimal, e.g. Z_3GHz RR does not suggest a ratio. Also their units is not dB as stated in the caption of Fig.1. (dB corresponds to 10 log10 of a UNITLESS quantity!!!); here you are defining a very specific unit (like the dBZ, you need to specify the units used for z and LWC).

Variable names are changed.

In the revision, the variables are defined as α and β

$$\alpha = 10 \log_{10}(Z_{DSD}^{3GHz}/RLWC) \quad \textbf{(A11)}$$

$$\beta = 10 \log_{10}(Z_{DSD}^{3GHz}/RR) \quad \textbf{(A12)}$$

The review's comments are right, the units of α and β should not be dB.
Instead of defining the units of α and β, as suggested, the units of RLWC and rain rate are specified in the captions of Figure A.

Estimation of Liquid Water Path below the Melting Layer in Stratiform Precipitation Systems using Radar Measurements during MC3E

Jingjing Tian[1], Xiquan Dong[1], Baike Xi[1], Christopher R. Williams[2], and Peng Wu[1]

[1]Department of Hydrology and Atmospheric Sciences, University of Arizona, Tucson, Arizona, USA

[2] Department of Ann and H.J. Smead Aerospace Engineering Sciences, University of Colorado Boulder

Manuscript Submitted to Atmospheric Measurement Techniques

Deleted: (October 30, 2018)

Corresponding author address: Dr. Xiquan Dong, The Department of Hydrology and Atmospheric Sciences, University of Arizona, 1133 E. James Rogers Way, Tucson, AZ 85721-0011.

Email: xdong@email.arizona.edu; Phone: 520-621-4652

Abstract

In this study, the liquid water path (LWP) below the melting layer in stratiform precipitation systems is retrieved, which is a combination of rain liquid water path (RLWP) and cloud liquid water path (CLWP). The retrieval algorithm uses measurements from the vertically pointing radars (VPRs) at 35 GHz and 3 GHz operated by the U.S Department of Energy Atmospheric Radiation Measurement (ARM) and National Oceanic and Atmospheric Administration (NOAA) during the field campaign Midlatitude Continental Convective Clouds Experiment (MC3E). The measured radar reflectivity and mean Doppler velocity from both VPRs and spectrum width from the 35 GHz radar are utilized. With the aid of the cloud base detected by ceilometer, the LWP in the liquid layer is retrieved under two different situations: (I) no cloud exists below the melting base, and (II) cloud exists below the melting base. In (I), LWP is primarily contributed from raindrops only, i.e., RLWP, which is estimated by analyzing the Doppler velocity differences between two VPRs. In (II), cloud particles and raindrops coexist below the melting base. The CLWP is estimated using a modified attenuation-based algorithm. Two stratiform precipitation cases (20 May 2011 and 11 May 2011) during MC3E are illustrated for two situations, respectively. With a total of 13 hours of samples during MC3E, statistical results show that the occurrence of cloud particles below the melting base is low (9%), however, the mean CLWP value can be up to 0.56 kg m^{-2}, which is much larger than the RLWP (0.10 kg m^{-2}). When only raindrops exist below the melting base, the averaged RLWP value is larger (0.32 kg m^{-2}) than the with cloud situation. The overall mean LWP below the melting base is 0.34 kg m^{-2} for stratiform systems during MC3E.

Deleted: 14

Deleted: 8

Deleted: 87

Deleted: 22

Deleted: 3

Deleted: 9

1. Introduction

Clouds in stratiform precipitation systems are important to the Earth's radiation budget. The vertical distributions of cloud microphysics, ice and liquid water content (IWC/LWC), determine the surface and top-of-the-atmosphere radiation budget and redistribute energy in the atmosphere (Feng et al., 2011; 2018). Also, stratiform precipitation systems are responsible for most tropical and midlatitude precipitation during summer (Xu, 2013). However, the representation of those systems in global climate and cloud-resolving models is still challenging (Fan et al., 2015). One of the challenges is due to the lack of comprehensive observations and retrievals of cloud microphysics (e.g. prognostic variables IWC and LWC) in stratiform precipitation systems. Liquid water path (LWP), defined as an integral of LWC in the atmosphere. It is a parameter used to provide the characterization of liquid hydrometeors in the vertical column of atmosphere and study clouds and precipitation. The estimation of LWC/LWP is one of the critical objectives of the US Department of Energy's (DOE) Atmospheric Radiation Measurement (ARM) Program (Ackerman and Stokes, 2003).

LWP can be retrieved using the ground-based MicroWave Radiometer (MWR) sensed downwelling radiant energy at 23.8 and 31.4 GHz (Liljegreen et al., 2001). In last two decades, ARM has been operating a network of 2-channel (23.8- and 31.4-GHz) ground-based MWR to provide a time series of LWP at the ARM Southern Great Plains (SGP) site (Cadeddu et al., 2013). Absorption-based algorithms using multichannels of MWRs have been widely used to retrieve cloud LWP (e.g., Liljegren et al. 2001; Turner, 2007), and they are known to be accurate methods to estimate LWP of nonprecipitating clouds with mean LWP error of 15 g m^{-2} (Crewell and Löhnert, 2003). However, in precipitating conditions, LWP retrieved from conventional

Deleted: are

Deleted: it is

MWR are generally not valid due to the violation of the Rayleigh assumption when large raindrops exist (e.g., Saavedra et al., 2012). In addition, large increase of brightness temperatures is measured as a result of the deposition of raindrops on the MWR's radome. Unfortunately, it is very hard to model and quantify this increase from rain layer on the radome (Cadeddu et al., 2017). This "wet-radome" issue largely inhibits the retrieving of LWPs using ground-based MWR during precipitation. Due to the limitations of retrieving LWP from MWR during precipitation, cloud and precipitation radars were used to simultaneously retrieve LWP (Matrosov, 2010).

In the precipitating system, the liquid water cloud droplets and raindrops often coexist in the same atmospheric layer (e.g., Dubrovina, 1982; Mazin, 1989; Matrosov, 2009, 2010), indicating that the LWP consists of both cloud liquid water path (CLWP) and rain liquid water path (RLWP). However, the discrimination between suspended small cloud liquid water droplets and precipitating large raindrops is a very challenging remote sensing problem. Even though the partitioning of LWP into CLWP and RLWP is important in cloud modeling (Wentz and Spencer, 1998; Hillburn and Wentz, 2008), there are few studies retrieved RLWP and CLWP simultaneously and separately (Saavedra et al., 2012; Cadeddu et al., 2017). Battaglia et al. (2009) developed an algorithm to retrieve RLWP and CLWP from the six Advanced Microwave Radiometer for Rain Identification (ADMIRARI) observables under rainy conditions. Saavedra et al (2012) developed an algorithm using both ADMIRARI and a micro rain radar to retrieve and analyze the CLWP and RLWP for midlatitude precipitation during fall. In addition to these RLWP and CLWP estimations mainly from passive microwave radiometers, there are several studies to estimate the LWP using active radar measurements only. Ellis and Vivekanandan (2011) developed an attenuation-based technique to estimate LWC, which is the sum of cloud

98 water contents (CLWC) and rain liquid water contents (RLWC), using simultaneous S- and Ka-
99 band scanning radars measurements. However, it is not always applicable of using these
100 techniques to retrieve LWC. If raindrop diameters are comparable to at least one of the radars'
101 wavelength, "Mie effect" will be included in the measured differential reflectivity, however this
102 "Mie effect" is not very distinguishable from differential attenuation effects (Tridon et al., 2013;
103 Tridon and Battaglia 2015).

104 Matrosov (2009) developed an algorithm to simultaneously retrieve CLWP and layer-
105 mean rain rate using the radar reflectivity measurements from three ground-based W-, Ka-, S-
106 bands radars. The CLWP were retrieved based on estimating the attenuation of cloud radar
107 signals compared to S-band radar measurements. Matrosov (2010) developed an algorithm to
108 estimate CLWP using a vertical pointing Ka-band radar and a nearby scanning C-band radar.
109 The layer-mean rain rate was first estimated with the aid of surface disdrometer, and then CLWP
110 was retrieved by subtracting the rain attenuation from total attenuation measured from two radars.
111 For the estimation of RLWP, Williams et al. (2016) developed a retrieval algorithm for rain drop
112 size distribution (DSD) using doppler spectrum moments observed from two collocated vertical
113 pointing radar (VPRs) at frequencies of 3 GHz and 35 GHz. The retrieved air motion and DSD
114 parameters were evaluated using the retrievals from a collocated 448-MHz VPR.

115 In this study, the CLWP retrieval algorithms in Matrosov (2009 and 2010) have been
116 modified given the available radar measurements, vertical pointing Ka- and S-band radars,
117 during the Midlatitude Continental Convective Clouds Experiment (MC3E) field campaign. For
118 the estimation of RLWP, we will basically follow the idea described in Williams et al. (2016) to
119 retrieve microphysical properties for raindrops. However instead of retrieving vertical air
120 motion and rain DSDs (Williams et al., 2016), this study aims at retrieving RLWCs, and then

Deleted: ,
Deleted: h

integrating RLWCs over the liquid layer to estimate RLWP. Overall, in this study, algorithms from three former publications are modified and combined to estimate the LWP in the stratiform precipitating systems.

The goals of this study are to retrieve the LWP, which includes both RLWP and CLWP retrievals using radars measurements, and tentatively answer two questions based on observations and retrievals in the stratiform precipitation systems during MC3E: (1) what is the occurrence of cloud below the melting base in the stratiform precipitation systems; (2) what are the values of simultaneous CLWP, RLWP and LWP, and how does CLWP or RLWP contribute to the LWP. Note that the CLWP and RLWP are constrained in a stratiform precipitation layer below the melting base and above the surface. The LWP estimations in this study are primarily aimed at stratiform precipitating events exhibiting melting-layer features from radar measurements with lower-to-moderate rain rates (RR < 10 mm hr^{-1}). The instruments and data used in this study are introduced in section 2. Section 3 describes the methods of retrieving LWP (both RLWP and CLWP). Section 4 illustrates two examples and followed by statistical results from more samples during MC3E. The last section gives the summary and conclusions. Acronyms and abbreviations are listed in Table 1.

2. Data

The MC3E field campaign, co-sponsored by the NASA Global Precipitation Measurement and the U.S. DOE ARM programs, was conducted at the ARM SGP (northern Oklahoma) during April-June 2011 to study convective clouds and improve model parametrization (Jensen et al., 2015). MC3E provided an opportunity to develop new retrieval methods to estimate cloud microphysics and precipitation properties in precipitation systems

(Giangrande et al., 2014; Williams, 2016; Tian et al., 2016; Tian et al, 2018). Several stratiform rain cases were observed by the VPRs during MC3E (as shown in Fig. 1). Distinct signatures of "bright band" are detected from VPRs. To retrieve LWP associated with stratiform precipitation, this study mainly uses the observations from two co-located VPRs operating at 3-GHz and 35-GHz at DOE ARM SGP Climate Research Facility.

Deleted: ing

2.1 Vertical Pointing Radars

The 3-GHz (S-band) VPR was deployed by NOAA Earth System Research Laboratory for the six-weeks during the MC3E. The NOAA 3-GHz VPR is a vertical pointing radar with 2.6° beamwidth monitoring precipitation overhead. This 3-GHz profiler bridges the gap between cloud radars, which are used to provide the structure of nonprecipitating clouds but are severely attenuated by rainfall, and precipitation radars, which, although unattenuated by rainfall, generally lack the sensitivity to detect more detailed cloud structure. The 3-GHz VPR observes the raindrops within the Rayleigh scattering regime and its signal attenuation are negligible through the rain. The temporal resolution of the profiles of Doppler velocity spectra is 7 seconds and the vertical resolution is 60 meters. The 3-GHz VPR operated in two modes: a precipitation mode and a low-sensitivity mode. The precipitation mode observations are used in this study.

The Ka-band ARM zenith radar (KAZR) is also a vertical pointing radar, operating at 35 GHz permanently deployed by DOE ARM at the SGP site. The KAZR measurements include reflectivity, vertical velocity, and spectral width from near-ground to 20 km. The KAZR data used in this study are the KAZR Active Remote Sensing of Clouds (ARSCL) product produced by the ARM (www.arm.gov). The KAZR-ARSCL corrects for atmospheric gases attenuation and velocity aliasing. By selecting the mode with the highest signal-to-noise ratio at a given point, data from two simultaneous operating modes (general and cirrus mode) are combined for

each profile to provide the "best estimates" of radar moments in the time-height fields. The vertical and temporal resolutions of KAZR-ARSCL product are 30 meters and 4 seconds, respectively. Since the 3-GHz and 35-GHz VPRs are independent radars with different dwell time and sample volumes (Williams et al., 2016), the radar observations are processed to 1-min temporal and 60-m vertical resolutions in this study.

2.2 Disdrometers

DOE ARM program maintains a suite of surface precipitation disdrometers. Measurements and estimations from the Distromet model RD-80 disdrometer and NASA two-dimensional video disdrometers (2DVD) deployed at the ARM SGP site are used in this study. The RD-80 disdrometer provides the most continuous raindrop size distribution (DSD) measurements at high spectral (20 size bins from 0.3 to 5.4 mm) and temporal resolutions (1 minute), and its minimal detectable precipitation amount is 0.006 mm hr^{-1}. From 2DVD, the rain DSDs are observed from 41 bins (0.1 - 10 mm), and its minimal detectable precipitation amount is 0.01 mm hr^{-1}. In addition to rain rate, the mean mass-weighted raindrop diameter (D_m) is also provided from 2DVD, which is used for evaluating retrieved D_m from radar measurements.

2.3 Ceilometer

A Vaisala laser ceilometer (CEIL) operates at the SGP Central Facility, sensing cloud presence up to a height of 7700m with 10-m vertical resolution. The laser ceilometer transmits near-infrared pulses of light, and the receiver detects the light scattered back by clouds and precipitation. It is designed to measure cloud-base height.

3. The Methodology of Liquid Water Path Estimation

As mentioned earlier, both RLWP and CLWP contribute to the LWP. With the aid of the cloud base height detected by ceilometer, LWP is retrieved under two different situations: (I) the cloud base is higher than the melting base and (II) the cloud base is lower than the melting base. For situation (I), there are almost no cloud droplets below melting base (CLWP = 0), and thus the LWP below the melting base is solely from raindrops. The LWP is calculated by integrating RLWCs over this layer. The RLWCs could be retrieved by analyzing the measured Doppler Velocity Differences ("*DVD Algorithm*") from two collocated VPRs. In situation (II), the small cloud droplets and large raindrops coexist below the melting base. Both raindrops and cloud particles contribute to LWP. RLWP will be still estimated using "*DVD Algorithm*". CLWP will be retrieved using an attenuation-based algorithm named as "*Attenuation Algorithm*". The algorithms for LWP estimation are summarized in a flowchart (Fig. 2).

3.1 Situation I (no cloud droplets exist below the melting base)

The algorithm from Williams et al. (2016) was developed based on an assumption that the 3-GHz VPR operates within the Rayleigh scattering regime for all raindrops, while the 35-GHz VPR operates within the Rayleigh scattering regime for small raindrops (diameters < ~1.3 mm) and non-Rayleigh scattering regime for larger raindrops (diameters ≥ ~1.3 mm). The different scattering regimes for the two operating frequencies result in different estimated radar moments. These estimated radar moments are in functions of rain microphysics. Thus, the rain microphysics could be retrieved with given measured radar moments. The details of this "*DVD Algorithm*" and uncertainty estimation are introduced in Appendix A.

3.2 Situation II (cloud particles and rain droplets coexist below the melting base)

In situation (II), substantial cloud particles exist below melting base, and both RLWP and CLWP retrievals are needed to estimate the LWP. The total two-way attenuation of 35-GHz

VPR signals, A (in decibels, dB), in a layer between the melting base and the cloud base, mainly consists of rain attenuation, liquid clouds attenuation, and gaseous attenuation. The total attenuation (A) are expressed as:

$$A = 2\,C\,R_m\,\Delta H + 2\,B\,CLWP + G. \quad (1)$$

R_m is layer-mean rain rate, and ΔH (km) is the thickness of the layer (Matrosov, 2009). G is the two-way attenuation/absorption from atmospheric gases, which is relatively small, and the absorption by gases has been already corrected in the KAZR ARSCL dataset and is assumed to be zero in our retrieval.

C and B are the coefficients for rainfall and cloud liquid water attenuation.

$$B = 0.0026\pi\lambda^{-1}\mathrm{Im}[-(m^2-1)(m^2+2)^{-1}], \quad (2)$$

where λ is the wavelength of Ka-band radar, and m is the complex refractive index of water. The unit of B is dB/g m^{-2}.

$$C = 0.27\,b, \quad (3)$$

where b is the correction factor considering raindrop fall velocities with changing air density.

$$b = (\rho_{am}/\rho_{a0})^{0.45}, \quad (4)$$

where ρ_{am} and ρ_{a0} are the mean air density in the rain layer and the density at normal atmospheric conditions.

Based on (1), CLWP can be written as:

$$CLWP = \frac{A - 2\,C\,R_m\,\Delta H - G}{2\,B} \quad (5)$$

The attenuation (A) is estimated by comparing the drop in Ka-band reflectivity with the un-attenuated S-band reflectivity through the cloud. Assuming the changes in reflectivity with altitude due to changes in raindrop size distributions with altitude are similar for Ka- and S-band

reflectivities, then the difference in reflectivities through the cloud is a proxy for attenuation. This can be expressed using

$$A \cong [Z_{Ka}(cloud\ base) - Z_{Ka}(melting\ base)] - [Z_S(cloud\ base) - Z_S(melting\ base)] \quad (6)$$

Notice that the absolute calibration of the radar was not important to the retrieval results since the retrieval of CLWP used S-Ka differential attenuation. This avoids the radar calibration (Tridon et al., 2015 and 2017), which is a serious issue limiting the accuracy of radar retrievals.

The R_m is estimated as:

$$R_m = \frac{\sum_{h0}^{MB} RR(h) \times \Delta h}{\Delta H}, \quad (7)$$

where Δh equals 60 meters and MB is the melting base and h_0 is the height of the lowest unsaturated KAZR rang gate (Matrosov, 2010). RRs in the layer between the melting base and the cloud base are calculated from the "*DVD algorithm*".

The uncertainties of retrieved CLWP are mainly due to the uncertainties of estimated R_m and observed total attenuation from VPRs. The value of B is on the order of 1 dB/kg m^{-2}. The uncertainty of retrieved CLWP would be ~ 0.25 kg m^{-2} with 0.5 dB uncertainty from measured radar reflectivity difference or ~ 0.5 kg m^{-2} for 1.0 mm hr^{-1} uncertainty from estimated layer-mean rain rate. Compared to the typical mean rain rate observed in the stratiform system (~ 2 - 4 mm hr^{-1}), 1.0 mm hr^{-1} represents a ~ 30% uncertainty. The uncertainty for CLWP retrievals is roughly estimated as ~ 0.56 kg m^{-2} (sqrt (0.25^2+0.5^2)) in this study. For reference, the expected uncertainty is reported as ~ 0.25 kg m^{-2} for typical rainfall rates (~ 3 - 4 mm hr^{-1}) in Matrosov (2009) retrieval method. More details of the estimation of CLWP uncertainties are in Appendix B.

4. Retrieval Results and Discussions

4.1 Case Studies

Deleted: s

Deleted: and CB are the melting base and the cloud base

Deleted: k

Deleted: ¶

Formatted: Font color: Text 1

Even though situation (I) is dominated (Fig. 1), especially in Case A, the ceilometer cloud base estimates can be lower than the melting base (Cases B to D). Two case studies (20 May 2011 and 11 May 2011) are given as examples to demonstrate the estimation of LWP in stratiform precipitation system for two different situations.

4.1.1 Case A

On 20 May 2011, an upper level low-pressure system at central Great Basin moved into the central and northern Plains, while a surface low pressure at southeastern Colorado brought the warm and moist air from the southern Plains to a warm front over Kansas. and a dry line extended southward from the Texas-Oklahoma. With those favorable conditions, a strong north-south oriented squall line developed over Great Plains and propagated eastward. The convection along the leading edge of this intense squall line exited the ARM SGP network around 11 UTC 20 May leaving behind a large area of stratiform rain (Case A in Fig. 1). This stratiform system passed over the ARM SGP site and observed by two VPRs, and disdrometers as shown in Figures 1a-1c. It clearly shows the 3-GHz radar echo tops are much lower than those from the 35 GHz VPR. Even though there is attenuation at 35-GHz by the raindrops and melting hydrometeors, the 35-GHz radar can still detect more small ice particles at near the cloud top. The "bright band", which occurs in a uniform stratiform rain region, is clearly seen from the 3-GHz VPR (a sudden increase and then decrease in radar reflectivity) but is not obvious from the 35-GHz VPR due to the non-Rayleigh scattering effects at 35 GHz (Sassen et al., 2005; Matrosov, 2008).

Figures 1a-1b clearly show that the ceilometer detected cloud base is in the middle of the melting layer, indicating almost no cloud particles below the melting layer and the LWP in the liquid layer equals to RLWP. The RLWP is retrieved using the "*DVD Algorithm*" introduced in

287 section 3.1 and Appendix A. Figure 3 shows an example of the DVD retrieval algorithm at
288 13:40 UTC on May 20, 2011. Radar reflectivity from 3 GHz, Doppler velocities from 3 GHz
289 and 35 GHz, and spectrum variance from 35 GHz are the inputs of DVD algorithm. The
290 Doppler velocity differences (3 GHz – 35 GHz) from the surface to 4 km are also plotted in Fig.
291 3d. The melting base is defined as the height of maximum curvature in the radar reflectivity
292 profile at 3 GHz (Fabry and Zawadzki, 1995), which is clearly seen at 2.5 km in Fig. 3. Below
293 2.5 km, the Doppler velocity differences between the two VPRs become relatively uniform,
294 indicating that the process of melting snow/ice particles into raindrops is completed. Retrieved
295 profiles of rain microphysical properties and their corresponding uncertainties (horizontal bars at
296 different levels) in the rain layer (0 – 2.5 km) are shown in Figs 3f-3h. In general, the retrieved
297 D_m values from the surface to 2.5 km are nearly a constant of ~2 mm (Fig. 3f), while the
298 retrieved RLWC and rain rate values slightly decrease from 2.5 km to the surface. One of the
299 highlights of this study is, in addition to the surface rain rate, which can usually be observed
300 using surface disdrometers, the vertical profiles of rain microphysical properties are retrieved.
301 These retrieved rain microphysical properties will shed light on the understanding of liquid cloud
302 and rain microphysical processes (like condensation, evaporation, autoconversion and accretion
303 etc.) in the models.

304 To evaluate the rain property retrievals, we compare the retrieved rain microphysical
305 properties, the D_m, and rain rate at the surface, with the surface disdrometers measurements (Fig.
306 4). The D_m values range from 1.0 to 2.5 mm during a 3.5-hr period with nearly identical mean
307 values of 1.79 mm and 1.81 mm from both retrievals and 2DVD measurements. There are large
308 variations for rain rates, ranging from 0 to 8 mm hr^{-1}, with means of 3.19, 3.17 and 2.88 mm hr^{-1},
309 respectively, from 2DVD, RD-80 and radar retrieval. The mean rain rates from 2DVD and RD-

80 measurements are almost the same although there are relatively large differences during certain time periods, while the retrievals from this study, on average, underestimate the rain rate by ~10% compared to the disdrometer measurements. More statistics (mean differences, their 95% confidence intervals of mean differences and root mean square errors) can be found in Table 2. Overall, the mean differences are within the retrieval uncertainties. The variation of RLWP (Fig. 4c) mimics the variation of retrieved rain rate in Fig. 4d. The mean value of RLWP is 0.55 kg m^{-2} for this case, which is also the LWP below the melting base.

4.1.2 Case B

On 11 May 2011, a surface cold front moved across the Oklahoma-Texas area and then convections were initiated. At 1600 UTC, a mesoscale convective system organized with a parallel stratiform precipitation region. Two-three hours later (~1830 UTC), the mesoscale convective system was transitioned to a trailing stratiform mode passed over the ARM SGP site. The large stratiform regions are observed by two VPRs and disdrometers as shown in Figs 1d-1f. Figures 1d-1f clearly show that the ceilometer detected cloud bases are lower than the melting bases occasionally. Under this situation, both RLWP and CLWP could contribute to the LWP below the melting base.

Firstly, the surface rain microphysics (D_m, RLWC, rain rate and RLWP) are retrieved using "*DVD Algorithm*". These rain property retrievals are compared with the surface disdrometers measurements (Fig. 5). The D_m values at the surface range from 0.90 to 2.30 mm during a 4.5-hr period with the mean values of 1.41 mm and 1.52 mm, respectively, from both retrievals and 2DVD measurements. The difference between the retrieval and 2DVD measurement may be due to different sampling volumes between radar and the surface disdrometer, as well as wind shear. The rain rates, in this case, vary quite large, ranging from

Deleted: relatedly

Deleted: 6

Deleted: 8

Deleted: 2

Deleted: 6

Deleted: 7

Deleted: To further investigate the difference, the measurements from five NASA 2DVDs located within 5 km away from VPRs are collected and processed. The almost same mean values and slight variation from 5 NASA 2DVDs measurements suggest that the difference between radar retrievals and the surface disdrometer measurements may be true, while averaging from more measurements can only smooth the variation. ¶
The mean rain rate values from five NASA 2DVDs and the surface disdrometer are very comparable, with a mean difference of 0.3 mm hr^{-1}. The almost same mean values between the surface disdrometer and 5 NASA 2DVDs measurements suggest that the DVDs apart within 5 km can capture very similar rain properties during a longer time period, such as 4.5 hours in this case, although there are some large differences from their point-to-point measurements. The rain rates

0.02 to 4.78 mm hr^{-1} with means of 1.36, 1.26 and 1.66 mm hr^{-1}, respectively from single 2DVD, RD-80, and our retrieval. It is found that, from both Case A and Case B, the mean value from RD-80 is smaller than that from 2DVD. This may be due to the different ranges of measurable drop sizes from two types of disdrometers (0.3 - 5.4 mm for RD 80, while 0.1 to 10 mm for 2DVD). More statistics can be also found in Table 2. Overall, the mean differences are still within the retrieval uncertainties for this case.

Secondly, the CLWP is retrieved using "Attenuation Algorithm" introduced in section 3.2. Figure 5c shows the time series of RLWP, CLWP and LWP retrievals. It is found that the CLWP values (when they exist) are usually larger than RLWP values in the same vertical column. When cloud droplets and raindrops coexist below the melting base, the mean values are 0.11 kg m^{-2} and 1.64 kg m^{-2} for RLWP and CLWP, and the corresponding LWP below the melting layer is 0.76 kg m^{-2}. While when only raindrops exist below the melting base, there is no CLWP (CLWP =0), and the RLWP and LWP are the same (with average of 0.34 kg m^{-2}). It is noticed that even though the occurrence of CLWP is low (11%) in this case, the value of CLWP can be very large when it exists, and it is about two times larger than the mean RLWP. The mean value of LWP is 0.37 kg m^{-2} for all the samples in Fig. 5c. The blue uncertainty bars in Figure 5c show the retrieved CLWP uncertainty with assuming both of the uncertainties of attenuation and total rain rate are 30% (Ua=Ur=30%). Due to the variations of the attenuation and total rain rate with time, the estimated uncertainties of CLWP varies point to point. More details about the estimation of CLWP are in Appendix B.

4.2 Statistical Results

Deleted: 9
Deleted: 81
Deleted: 64
Deleted: 98
Deleted: 3
Deleted: 00
Deleted: 1.31
Deleted: 3
Deleted: 2
Deleted: 45

Box and whisker plots of retrieved RLWP, CLWP and LWP for situations (I), (II) and all samples during MC3E are shown in Fig. 6. The horizontal orange and red dashed lines indicate the median and mean, boundaries of the box represent the first and third quartiles, and the whiskers are the 10th- and 90th -percentiles. During MC3E, a total of 13 hours of stratiform rain were observed by VPRs at the ARM SGP Climate Research Facility, in which 91% and 9% the samples are categorized into the situations (I) and (II), respectively. The mean RLWPs are 0.32 kg m^{-2} and 0.10 kg m^{-2} for the situations (I) and (II). There are a substantial amount of small cloud droplets sustaining in the rain layer and having not yet converted to larger raindrops, which may partially explain smaller RLWP in the situation (II). The mean value of surface rain rate is 2.06 mm hr^{-1} when cloud droplets exist, which is also smaller than the mean value (2.38 mm hr^{-1}) in the rain-only situation. The mean CLWP in the situation (II) is as large as ~0.56 kg m^{-2} even though their occurrence is very low (9%), which is much larger than mean RLWP in the liquid layer. The LWP from the situation (II) (0.66 kg m^{-2}) is much larger than the mean LWP from the situation (I) (0.32 kg m^{-2}), which is primarily contributed by cloud droplets. The overall mean LWP for stratiform rain during MC3E is 0.34 kg m^{-2}.

We also processed the ARM MWR retrieved LWPs during MC3E and compared them with our retrievals as illustrated in Fig. 7a. The corresponding LWP uncertainties are also provided as the grey error bar for each retrieval with rain rate indicated by colors. It is notice that the MWR has no LWP estimation when the rain rate is large. The MWR-retrieved LWPs increase with increased rain rate, and much larger than the new LWP retrievals at high rate rates. The newly retrieved LWPs weakly correlate with rain rates, and most values are less than 1.0 kg m^{-2}, especially at high rain rates. The MWR retrieved LWPs increase with rain rate generally. The increase of retrieved LWP with rain rate from MWR is possibly due to the "wet radome" effect

Deleted: 4

Deleted: 2

Deleted: 8

Deleted: 3

Deleted: 22

Deleted: e

Deleted: 1.78

Deleted: 06

Deleted: 87

Deleted: 8

Deleted: The ratio of RLWP and CLWP ranges from 4:1 to 2:1 for precipitating shallow marine clouds reported at Lebsock et al. (2011), while our results from MC3E do not seem to have a clear linear relationship between CLWP and RLWP (figure is not shown).…

Deleted: 9

Deleted: ¶

Formatted: Indent: First line: 0"

Formatted: Font: Not Bold

Formatted: Font: Not Bold

(Cadeddu et al., 2017). In addition to the issue from standing water on the radome, the extinctions due to raindrops also affect MWR retrievals. The extinction for rain is much larger than that for cloud (Sheppard, 1996), and thus, the small amount of rain water could enhance the measured brightness temperature significantly. More details of extinctions and brightness temperature calculations are shown in Appendix B. Statistical results of the retrieved LWPs from this study and MWR are averaged for each measured rain rate bins (bin size = 0.25 mm hr^{-1}). The differences of LWPs from MWR and this study are shown in Fig. 7b. The LWP differences increase with increased rain rate. The LWP differences between MWR retrieval and this study could be caused by the following reasons. 1) MWR-retrieved LWP represents the entire vertical column (RWLP and CLWP below melting layer, large water coated ice particles in the melting layer and supercooled LWCs above the melting layer), while our retrieval only represents the LWP below the melting base. As Battaglia et al (2003) pointed out the brightness temperature generally increases if mixed-phase precipitation is included. 2) The MWR radome was wet during the raining periods and the deposition of raindrops on the radome can cause a large increase in the measured brightness temperatures (Cadeddu et al., 2017). 3) Large extinctions from rain drops would affect MWR retrievals. 4) Uncertainties exist in the retrieved LWP from this study.

5. Summary and Conclusions

LWP is a critical parameter for studying clouds, precipitation, and their life cycles. LWP can be retrieved from microwave radiometer measured brightness temperatures during cloudy and light precipitation conditions. However, MWR-retrieved LWPs are questionable under moderate and heavy precipitation conditions due to the "wet radome" and large extinction effects

Deleted: Statistical results of the retrieved LWPs from this study and MWR are averaged for each measured rain rate bins (bin size = 0.25 mm hr^{-1}). When the rain rate is greater than ~ 6mm hr^{-1}, there are no MWR LWP retrievals. Fig. 7b shows that the MWR retrieved LWPs, as expected, monotonically increase with rain rate, which is possible due to the "wet radome" effect (Cadeddu et al., 2017). "Wet radome" is a particularly complicated situation because the standing water often looks physically like a layer and less like a collection of drops, making the MWR overestimate LWPs (personal communication with Dave Turner, 2018), and so far, no effective method was found to solve this problem (Cadeddu et al., 2017). ¶
In addition to the issue from standing water on the radome, the scattering effects due to raindrops also affect MWR retrievals. Two general retrieval methods are commonly used to retrieve LWP from the observed brightness temperatures: statistical methods (Liljegren et al., 2001) and physical retrievals (Turner et al, 2007). No matter which retrieval is used, the radiative transfer code usually only models the absorptions from atmospheric gases and cloud liquid water. The scattering effect is not taken into consideration during the retrieval, that is, it is under the assumption that the brightness temperature is primarily due to the emission of cloud droplets in the MWR retrieval. Even small drizzle particles still have a scattering effect, which could contribute higher brightness temperature measured by MWR and result in larger retrieved LWPs than the "true" LWPs. Therefore, the MWR retrieved LWPs are most likely overestimated for precipitating clouds.¶
In this study, we mainly focus on the stratiform rain systems with mean rain rates of 2-4 mm hr^{-1}. The scattering effect for large raindrops is more significant than drizzles. Sheppard (1996) examined the effect of raindrops on MWR brightness temperature measurements at 31 GHz and found that cloud absorption coefficient is only ~2/3 of rain absorption coefficient, however, the scattering effect of raindrops is not insignificant where its scattering coefficient is about half of cloud absorption coefficient. Thus, MWR measured brightness temperatures for precipitating clouds would be higher, due to the scattering by raindrops, than those for non-precipitating clouds, and then result in higher LWPs than the 'true" LWPs. The differences of LWPs from MWR and this study are shown in Fig. 7c. The LWP differences increase almost linearly with increased rain rate. The differences could be due to (1) MWR retrieved LWP represents the whole vertical column (RWLP and CLWP below melting layer, large water coated ice particles in the melting layer and supercooled LWCs above the melting layer), while our retrieval only represent the LWP below the melting base; (2) existing uncertainty in retrieved LWP from this study (~0.6 kg m^{-2} when includeing CLWP estimates). …

Formatted: Font color: Black

Formatted: Font: (Default) Times New Roman, (Asian) SimSun, Bold, Font color: Auto

Deleted: non-Rayleigh scattering

caused by large raindrops. LWPs below the melting base in stratiform precipitation systems are estimated, which include both RLWP and CLWP. The measurements used in this study are mainly from two VPRs, 35-GHz from ARM and 3-GHz from NOAA during the MC3E field campaign.

In this study, the microphysical properties of raindrops, such as D_m, RLWC (and RLWP), and RR, are estimated following the method described in Williams et al. (2016) using measurements from co-located Ka- and S-band radars VPRs. The retrieved rain microphysical properties are validated by the surface disdrometer measurements. Instead of retrieving vertical air motion and rain DSDs (Williams et al., 2016), this study aims at retrieving RLWCs and then integrating RLWCs over the liquid layer to estimate RLWP. The CLWP is retrieved based on the modifications of the methods in Matrosov (2009 and 2010) with available radar measurements, vertical pointing Ka- and S-band VPRs, during the MC3E field campaign.

The applicability of retrieval methods is illustrated for two stratiform precipitation cases (20 May 2011 and 11 May 2011) observed during MC3E. Statistical results from a total of 13 hours samples during MC3E show that the occurrence of cloud droplets below the melting base is low (9%), while the CLWP value can be up to 0.56 kg m^{-2}, which is much larger than the RLWP (0.10 kg m^{-2}). When only raindrops exist below the melting base, the averaged RLWP value is 0.32 kg m^{-2}, which is much larger than the mean RLWP in the cloud droplets and raindrops coexisted situation.

Reliable retrievals of RLWC and RLWP are critical for model evaluation and improvement, as RLWC (rain mixing ratio) is an important prognostic variable in weather and climate models. Furthermore, the retrievals in the whole rain layer would be useful to understand the microphysical processes (i.e., condensation, evaporation, autoconversion, and

Deleted: 4

Deleted: 8

Deleted: 87

Deleted: 22

Deleted: 3

accretion etc.) and have great potential to improve model parametrizations in the future. Overall, the LWP (CLWP and RLWP) retrievals derived in this study can be used to evaluate the models that separately predict cloud and precipitation, and contribute comprehensive information to study cloud-to-precipitation transitions.

Deleted: separately

Appendix A: Doppler Velocity Differences Algorithm ("*DVD Algorithm*")

Retrieving RLWC and other rain microphysical properties (i.e., drop size and rain rate) is based on the mathematics of DSD radar reflectivity-weighted velocity spectral density S_{DSD}^{λ} [(mm^6 m^{-3}) (m s^{-1})$^{-1}$], which is a product of radar raindrop backscattering cross section $\sigma_b^{\lambda}(D)$ (mm^2) and DSD number concentration $N_{DSD}(D)$ (mm^{-1} m^{-3}):

$$S_{DSD}^{\lambda}(v_z) = [\frac{\lambda^4}{\pi^5 |K_w|^2}\sigma_b^{\lambda}]N_{DSD}(D)\frac{dD}{dv_z}. \quad (A1)$$

The $\frac{dD}{dv_z}$ [mm (m s^{-1})$^{-1}$] is used as a coordinate transformation from diameter to velocity, where v_z (m s^{-1}) is the raindrop terminal velocity of diameter D (mm) at altitude z. λ is the wavelength of radar. $|K_w|^2$ equals 0.93 and it is the dielectric factor.

The $N_{DSD}(D)$ can be expressed as a normalized gamma shape distribution with a three parameters (Leinonen et al., 2012):

$$N_{DSD}(D; N_w, D_m, \mu) = N_w f(D; D_m, \mu), \quad (A2)$$

where

$$f(D; D_m, \mu) = \frac{6}{4^4}\frac{(\mu+4)^{(\mu+4)}}{\Gamma(\mu+4)}(\frac{D}{D_m})^{\mu}\exp[-(\mu+4)\frac{D}{D_m}]. \quad (A3)$$

N_w is the scaling parameter, μ is a shape parameter, $\Gamma(x)$ is the Euler gamma function, and D_m is a mean mass-weighted raindrop diameter estimated from the ratio of the fourth to third DSD moments:

$$D_m = \frac{M_4}{M_3} = \frac{\int_{D_{min}}^{D_{max}} N_{DSD}(D) D^4 dD}{\int_{D_{min}}^{D_{max}} N_{DSD}(D) D^3 dD}. \quad (A4)$$

where D_{min} and D_{max} represent the minimum and maximum diameters in the distribution, respectively.

The intrinsic (non-attenuation) reflectivity factor and the mean velocity and the spectrum variance are the zeroth, first, and second reflectivity-weighted velocity spectrum moments :

$$Z_{DSD}^{\lambda} = \sum_{v_{min}}^{v_{max}} S_{DSD}^{\lambda}(v_i) \Delta v \quad (A5)$$

$$v_{DSD}^{\lambda} = \frac{\sum_{v_{min}}^{v_{max}} S_{DSD}^{\lambda}(v_i)\, v_i\, \Delta v}{Z_{DSD}^{\lambda}} \quad (A6)$$

$$SV_{DSD}^{\lambda} = \frac{\sum_{v_{min}}^{v_{max}} (v_i - v_{DSD}^{\lambda})^2 S_{DSD}^{\lambda}(v_i)\, \Delta v}{Z_{DSD}^{\lambda}}. \quad (A7)$$

where v_i is the discrete velocities and Δv is velocity resolution in the integration.

The Doppler Velocity Difference (DVD) is defined as

$$DVD = v_{DSD}^{3\ GHz} - v_{DSD}^{35\ GHz}. \quad (A8)$$

Note that both DVD and SV are dependent on DSD parameters (D_m and μ) only.

The RLWC and rain rate (RR) can also be described using the DSD:

$$RLWC(g\ m^{-3}) = \frac{\pi}{6} 10^{-3} \sum_{D_{min}}^{D_{max}} N_{DSD}(D, N_w, D_m, \mu) D_i^3 \Delta D \quad (A9)$$

$$RR(mm\ hr^{-1}) = \frac{6\pi}{10^4} \sum_{D_{min}}^{D_{max}} N_{DSD}(D, N_w, D_m, \mu) D_i^3 v_z(D_i) \Delta D. \quad (A10)$$

In addition, there are two newly defined radar-related parameters (α and β), which are also dependent on D_m and μ only:

$$\alpha = 10 \log_{10}(Z_{DSD}^{3GHz}/RLWC) \quad (A11)$$

$$\beta = 10 \log_{10}(Z_{DSD}^{3GHz}/RR) \quad (A12)$$

In this study, four variables, DVD, SV at 35 GHz (SV_{35GHz}), α and β, are pre-calculated using different groups of D_m and μ values, and then these values are stored in look-up tables

Deleted: In addition, there are two newly defined radar-related parameters ($Z_{3GHZ}LWC$ and $Z_{3GHZ}RR$), which are also dependent on D_m and μ only: ¶
$Z_{3GHZ}LWC=10 \log_{10}(Z_{DSD}^{3GHz}/RLWC)$ →→→→(A11)¶
$Z_{3GHZ}RR=10 \log_{10}(Z_{DSD}^{3GHz}/RR)$ →→→→(A12)¶

Deleted: $Z_{3GHZ}LWC$ and $Z_{3GHZ}RR$

582 (LUTs). Raindrop backscattering cross sections are calculated using the T-matrix with different
583 temperatures and oblate raindrop axis ratios (Leinonen, 2014). LUT examples are illustrated in
584 Fig. A as functions of DVD and SV_{35GHz}. If we assume that the observed radar Doppler velocity
585 difference and spectrum variance from the 35-GHz radar is equal to the DSD velocity difference
586 and variance (DVD and SV_{35GHz}), the measured Doppler velocity difference and spectrum
587 variance at 35-GHz can determine a solution for D_m from the LUT (Fig. A(a)). Similarly, a value
588 of Z_{3GHZ}LWC (or Z_{3GHZ}RR) can be found with measured DVD and SV_{35GHz} using the LUT in Fig.
589 A(b) (or Fig. A(c)). Then RLWC (or RR) can be estimated using (A11) (or (A12)) with
590 measured reflectivity at 3-GHz (Z_{3GHZ}).

591 The observed radar Doppler velocity difference can be assumed to be equal to the DSD
592 velocity difference for two reasons: (1) even though the radar observed Doppler velocity
593 spectrum can be broaden by the air motion, this spectrum broadening variance is small (within
594 2%) relative to the DSD velocity spectrum because of the narrow beamwidth (0.2^o) of KAZR
595 and (2) spectrum broadening is symmetric, which does not affect the first spectrum moment and
596 the DSD mean Doppler velocity only shifts due to the air motion. Therefore, the measured
597 differences of Doppler velocity between the 3-GHz and 35- GHz radars vertical pointing
598 observations are independent of air motion and can be assumed to be the same as DVD from
599 (A8). The validity of such an assumption is fully discussed in Williams et al. (2016).

600 The variabilities of 3-GHz and 35-GHz VPR observations within each 1-minute/60-meter
601 bin are regarded as the measurement uncertainties and will be propagated through the retrieval to
602 produce retrieval uncertainties. The retrieval uncertainties are estimated follow two steps: (1)
603 construct a distribution of input radar measurements. For example, the temporal resolution for 3-
604 GHz VPR is seven seconds, thus there are about nine radar reflectivities observed for one minute.

A normal distribution is generated first using the mean and standard deviations of these nine observed radar reflectivities for this 1-min/60-m resolution/bin. (2) repeat the DVD retrievals using samplings from distributions of all input measurements. We randomly select 100 groups of members from those (DVD, SV_{35GHz}, Z_{3GHZ}) normal distributions to form 100 realizations, and then produce 100 separate output estimates. The mean and standard deviation of the 100 solutions are regarded as the final retrieval and the retrieval uncertainty.

The uncertainties of RLWP are estimated based on the uncertainties of RLWC. More specifically, we first estimated the RLWC uncertainties at each height level, and then we calculated the ratios of RLWC uncertainties to mean retrieved RLWCs at each height level, which represent percentage values of retrieval uncertainties. Finally, we calculated the mean ratio of the uncertainties in the whole liquid layer below melting base and regarded this mean ratio as the uncertainty of RLWP.

Formatted: Font: Not Bold

It is noted that the uncertainty here only considers estimates of instrument noise, not the uncertainties associated with assumptions used in the retrieval. For example, the gamma size distribution used in (A2) is an approximation which may introduce error into the retrieval. However, it is very difficult to quantify this type of retrieval uncertainty. In this study, we further compared our retrievals with independent surface disdrometers measurements to estimate the uncertainties of retrievals. Also, when both radars are observing at Rayleigh scattering for small raindrops, the reflectivity-weighted radial velocities for these particles should be the same. In order to have a difference in radial velocity during the retrieval, large droplets must exist. The maximum diameters in drop size distribution measured from disdrometer for all the stratiform cases during MC3E are investigated. It is found that the occurrence of small-droplets-only (maximum diameter <1.3 mm) is very low (less than 3%). Thus, it will not have a significant

impact on the retrieval results. Notice that this algorithm is not suitable for strong convective rain due to the wind shear and strong turbulence as well as severe attenuation and extinction of the Ka-band radar signal.

Appendix B: CLWP Uncertainty

CLWP can be simplified and estimated as following equation:

$$\mathrm{CLWP} = \frac{\mathrm{A} - 2\,\mathrm{C}\,R_{total}}{2\,\mathrm{B}} \quad \text{(B1)}$$

The attenuation (A) is estimated by comparing the drop in Ka-band reflectivity with the un-attenuated S-band reflectivity. The rain attenuation is estimated by the rain attenuation coefficient (C) multiplied by the total rain rate (R_{total}). C and B are the coefficients of rain and cloud water attenuation with values of ~ 0.26 dB /km /mm hr^{-1} and ~ 0.87 dB / kg m^{-2}, respectively. The influence of temperature uncertainty in B on the retrieval error is minor compared to the uncertainties of the total attenuation (A) and total rain rate (R_{total}) (Matrosov 2010). The uncertainty of CLWP is calculated as

$$\Delta CLWP = \sqrt{\left(\frac{\partial CLWP}{\partial A} \times \Delta \mathrm{A}\right)^2 + \left(\frac{\partial CLWP}{\partial R_{total}} \times \Delta R_{total}\right)^2} \quad \text{(B2)}$$

$$\Delta CLWP = \sqrt{\left(\frac{1}{2B} \times \mathrm{A} \times \mathrm{Ua}\right)^2 + \left(-\frac{C}{B} \times R_{total} \times \mathrm{Ur}\right)^2} \quad \text{(B3)}$$

For given uncertainties of attenuation (Ua) and total rain rate (Ur), the uncertainty of CLWP can be calculated based on equation (B3).

Formatted: Line spacing: Double

Formatted: Font: Not Bold

Appendix C: Calculations of Extinction and Brightness Temperature at Microwave Radiometer Channels

To better explain the "overestimation" issue of retrieved LWP from microwave radiometer, several examples are given in this appendix. Firstly, we calculated the extinction cross section per volume as a function of the drop equivolume diameter for the two frequencies in MWR (23.8 GHz and 31.4 GHZ) with a T-matrix method (Figure B). It is clearly shown that the extinction cross section is increasing with the diameter when the diameter is smaller than 3 mm. This indicates the extinction (cross section) for rain drops (diameter > ~ 50 um) is much larger than that for cloud droplets (diameter < ~50 um). Secondly, we calculated the extinction coefficient as a function of RLWC for populations with three different drop size distributions (DSDs). The DSDs are modeled according to the exponential Marshall and Palmer (MP) distribution $N(D) = N_0 e^{-\Lambda D}$, where N_0=8000 m^{-3} mm^{-1}. N_0 is changed to 4000 and 32000 m^{-3} mm^{-1} to represent thunderstorm and drizzle DSDs. More details of the DSDs please see Battaglia et al. (2009). Figure C clearly shows the extinctions of cloud and rain also is DSD-dependent. For example, at 31.4 GHz, even though the RLWC is the same, the extinctions are much larger from the precipitation with the thunderstorms and MP DSDs than the extinctions from light precipitation with the drizzle DSD.

In addition, the brightness temperatures at 23.8 and 31.4 GHz channels are calculated using the MicroWave Radiative Transfer (MWRT) model. Five different sensitivity tests are generated with five combinations of CLWP and RLWP values (Table A). Table A lists the results and clearly demonstrates that the brightness temperatures in channels increase with increased cloud water amount (larger CLWP) and the rain water amount (larger RLWP). Comparing the results from test #2 and #3, it is clearly seen that the brightness temperatures

Formatted: Indent: First line: 0.5", Don't adjust right indent when grid is defined, Don't snap to grid

672 contributed by rain drops are 31 and 51 K more than that contributed by cloud droplets at the
673 frequencies of 23.8 and 31.4 GHz, even though their LWPs are the same (1 kg m^{-2}) in these two
674 tests.
675
676 **Acknowledgments:** J. Tian and X. Dong are supported by DOE CMDV project under grant DE-
677 SC0017015 at the University of Arizona, and B. Xi is supported by NASA CERES project under
678 grant NNX17AC52G at the University of Arizona. C. R. Williams is supported by DOE ASR
679 project under grant DE-SC0014294. Special thanks to Dr. Sergey Matrosov from NOAA Earth
680 System Research Laboratory (ESRL) for his suggestions. Special thanks to Michael Jensen, PI
681 of MC3E. Aircraft in situ measurements are processed using data from
682 https://ghrc.nsstc.nasa.gov/pub/fieldCampaigns/gpmValidation/mc3e/, can also be obtained from
683 Xiquan Dong (xdong@email.arizona.edu). NOAA vertical profile radar datasets are publically
684 available in the DOE archives (http://iop.archive.arm.gov/arm-iop/2011/sgp/mc3e/williams-
685 s_band/).
686

687 **References**

688 Ackerman, T. P., and Stokes, G. M: The Atmospheric Radiation Measurement Program. Phys.
689 Today, 56,38–44, doi:10.1063/1.1554135, 2003
690 Battaglia, A., Saavedra, P., T. Rose, and Simmer, C.: Characterization of precipitating clouds by
691 ground-based measurements with the triple-frequency polarized microwave radiometer
692 ADMIRARI, J. Appl. Meteorol., 49(3), 394–414, 2009
693 Battaglia, A., C. Kummerow, D. Shin, and C. Williams, 2003: Constraining Microwave
694 Brightness Temperatures by Radar Brightband Observations. J. Atmos. Oceanic
695 Technol., 20, 856–871, https://doi.org/10.1175/1520
696 0426(2003)020<0856:CMBTBR>2.0.CO;2
697 Cadeddu, M. P., Liljegren, J. C., and Turner, D. D.: The Atmospheric radiation measurement
698 (ARM) program network of microwave radiometers: instrumentation, data, and retrievals,
699 Atmos. Meas. Tech., 6, 2359-2372, https://doi.org/10.5194/amt-6-2359-2013, 2013
700 Cadeddu, M. P., Marchand, R., Orlandi, E., Turner, D. D. and Mech, M. (2017). Microwave
701 Passive Ground-Based Retrievals of Cloud and Rain Liquid Water Path in Drizzling
702 Clouds: Challenges and Possibilities, IEEE Transactions on Geoscience and Remote
703 Sensing, vol. 55, no. 11, pp. 6468-6481, doi: 10.1109/TGRS.2017.2728699
704 Crewell, S., and Löhnert, U. (2003). Accuracy of cloud liquid water path from ground-based
705 microwave radiometry 2. Sensor accuracy and synergy, Radio Sci., 38, 8042,
706 doi:10.1029/2002RS002634, 3.
707 Dubrovina, L. S.: Cloudness and precipitation according to the data of airplane soundings,
708 Gidrometeoizdat, Leningrad (in Russian), 218 pp,1982

709 Ellis, S. M., and Vivekanandan, J.: Liquid water content estimates using simultaneous S and K_a
710 band radar measurements, Radio Sci., 46, RS2021, doi:10.1029/2010RS004361, 2011
711 Fabry, F. and Zawadzki, I.: Long-Term Radar Observations of the Melting Layer of Precipitation
712 and Their Interpretation. J. Atmos. Sci., 52, 838–851, https://doi.org/10.1175/1520-
713 0469(1995)052<0838:LTROOT>2.0.CO;2, 1995
714 Fan, J., Liu, Y.-C., Xu, K.-M., North, K., Collis, S., Dong, X, and Ghan, S. J.: Improving
715 representation of convective transport for scale-aware parameterization:1. Convection
716 and cloud properties simulated with spectral bin and bulk microphysics, Journal of
717 Geophysical Research: Atmosphere, 120, 3485–3509,
718 https://doi.org/10.1002/2014JD022142, 2015
719 Feng, Z., Dong, X. Q., Xi, B. K., Schumacher, C., Minnis, P., and Khaiyer, M.: Top-of-
720 atmosphere radiation budget of convective core/stratiform rain and anvil clouds from
721 deep convective systems. Journal of Geophysical Research, 116, D23202. https://doi.org/
722 10.1029/2011JD016451, 2011
723 Feng, Z., Leung, L. R., Houze, R. A., Jr., Hagos, S., Hardin, J., Yang, Q., Han, B. and Fan, J.:
724 Structure and evolution of mesoscale convective systems: Sensitivity to cloud
725 microphysics in convection-permitting simulations over the United States. Journal of
726 Advances in Modeling Earth Systems, 10, 1470–1494.
727 https://doi.org/10.1029/2018MS001305, 2018
728 Giangrande, S. E., Collis, S., Theisen, A. K., and Tokay, A.: Precipitation estimation from the
729 ARM distributed radar network during the MC3E campaign, J. Appl. Meteor. Climatol.,
730 doi:10.1175/JAMC-D-13-0321.1, 2014

Deleted: ol

732 Jensen, M.P., Petersen, W. A., Bansemer, A., Bharadwaj, N., Carey, L. D., Cecil, D. J, and
733 Zipser, E. J.: The Midlatitude Continental Convective Clouds Experiment (MC3E),
734 Bulletin of the American Meteorological Society. 151221073208006.
735 https://doi.org/10.1175/BAMS-D-14-00228.1, 2015
736 Leinonen, J., Moisseev, D., M. Leskinen, M., and W.A. Petersen, W.A.: A Climatology of
737 Disdrometer Measurements of Rainfall in Finland over Five Years with Implications for
738 Global Radar Observations. J. Appl. Meteor. Climatol., 51, 392–404,
739 https://doi.org/10.1175/JAMC-D-11-056.1, 2012
740 Leinonen, J.: High-level interface to T-matrix scattering calculations: architecture, capabilities
741 and limitations, Opt. Express, vol. 22, issue 2, 1655-1660 doi: 10.1364/OE.22.001655,
742 2014
743 Liljegren, J. C., Clothiaux, E. E., Mace, G. G., Kato, S., and Dong, X.: A new retrieval for cloud
744 liquid water path using a ground-based microwave radiometer and measurements of
745 cloud temperature, J. Geophys. Res., 106(D13), 14485–14500,
746 doi:10.1029/2000JD900817, 2001
747 Lebsock, M.D., L'Ecuyer, T.S. and Stephens, G.L.: Detecting the Ratio of Rain and Cloud
748 Water in Low-Latitude Shallow Marine Clouds. J. Appl. Meteor. Climatol., 50, 419–432,
749 https://doi.org/10.1175/2010JAMC2494.1, 2011
750 Matrosov, S. Y.: Assessment of radar signal attenuation caused by the melting hydrometeor layer.
751 IEEE Trans. Geo Sci. Remote Sens.,46,1039–1047 doi: 10.1109/TGRS.2008.915757,
752 2008

753 Matrosov, S. Y.: A method to estimate vertically integrated amounts of cloud ice and liquid and
754 mean rain rate in stratiform precipitation from radar and auxiliary data, J. Appl. Meteor.
755 Climatol., 48, 1398–1410, doi:10.1175/2009JAMC2196.1, 2009
756 Matrosov, S. Y.: Synergetic use of millimeter- and centimeter-wavelength radars for retrievals of
757 cloud and rainfall parameters, Atmos. Chem. Phys., 10, 3321-3331,
758 https://doi.org/10.5194/acp-10-3321-2010, 2010
759 Mazin, I. P. (Ed.): Clouds and the Cloudy Atmosphere. Gidrometeoizdat, Leningrad, 648 pp,
760 1989.
761 Saavedra, P., Battaglia, A., and Simmer, C.: Partitioning of cloud water and rainwater content by
762 ground-based observations with the Advanced Microwave Radiometer for Rain
763 Identification (ADMIRARI) in synergy with a micro rain radar, J. Geophys. Res., 117,
764 D05203, doi:10.1029/2011JD016579, 2012
765 Sassen, K., Campbell, J. R., Zhu, J., Kollias, P., Shupe, M., and Williams, C.: Lidar and Triple-
766 Wavelength Doppler Radar Measurements of the Melting Layer: A Revised Model for
767 Dark- and Brightband Phenomena. J. Appl. Meteor., 44, 301–312,
768 https://doi.org/10.1175/JAM-2197.1, 2005
769 Sheppard, B.E.: Effect of Rain on Ground-Based Microwave Radiometric Measurements in the
770 20–90-GHz Range. *J. Atmos. Oceanic Technol.*, 13, 1139–1151,
771 https://doi.org/10.1175/1520-0426(1996)013<1139:EOROGB>2.0.CO;2, 1996
772 Tian, J., Dong, X., Xi, B., Wang, J., Homeyer, C. R., McFarquhar, G. M., and Fan J.: Retrievals
773 of ice cloud microphysical properties of deep convective systems using radar
774 measurements, Journal of Geophysical Research: Atmosphere., 121,10 ,820–10,839,
775 https://doi.org/10.1002/2015JD024686, 2016

Deleted: J. Appl. Meteorol.,

Formatted: Font: Not Italic

777 Tian, J., Dong, X., Xi, B., Minnis, P., Smith, W. L., Jr, Sun-Mack, S., … Wang, J.: Comparisons
778 of ice water path in deep convective systems among ground-based, GOES, and CERES-
779 MODIS retrievals. Journal of Geophysical Research: Atmospheres, 123, 1708–1723.
780 https://doi.org/10.1002/2017JD027498, 2018
781 Tridon, F., and Battaglia, A.: Dual-frequency radar Doppler spectral retrieval of rain drop size
782 distributions and entangled dynamics variables, J. Geophys. Res. Atmos., 120, 5585–
783 5601, doi:10.1002/2014JD023023, 2015
784 Tridon, F., Battaglia, A., and Kollias, P.: Disentangling Mie and attenuation effects in rain using
785 a Ka-W dual-wavelength Doppler spectral ratio technique, Geophys. Res. Lett., 40, 5548
786 5552, doi:10.1002/2013GL057454, 2013
787 Tridon, F., Battaglia, A., Luke, E., and Kollias, P.: Rain retrieval from dual-frequency radar
788 Doppler spectra: validation and potential for a 25 midlatitude precipitating case-study,
789 Quarterly Journal of the Royal Meteorological Society, 143, 1364–1380, 2017.
790 Turner, D. D., Clough, S. A., Liljegren, J. C., Clothiaux, E. E., Cady-Pereira, K. E., and Gaustad,
791 K. L.: Retrieving liquid water path and precipitable water vapor from the Atmospheric
792 Radiation Measurement (ARM) microwave radiometers. IEEE Trans. Geosci. Remote
793 Sens., 45, 3680–3690, 2007
794 Wentz, F.J. and Spencer, R.W.: SSM/I Rain Retrievals within a Unified All-Weather Ocean
795 Algorithm. J. Atmos. Sci., 55, 1613–1627, https://doi.org/10.1175/1520-
796 0469(1998)055<1613:SIRRWA>2.0.CO;2, 1998
797 Williams, C. R.: Reflectivity and liquid water content vertical decomposition diagrams to
798 diagnose vertical evolution of raindrop size distributions, J. Atmos. Oceanic Technol.,
799 doi:10.1175/JTECH-D-15-0208.1, 2016

800 Williams, C. R., Beauchamp, R. M., and Chandrasekar, V.: Vertical air motions and raindrop
801 size distributions estimated from mean Doppler velocity difference from 3- and 35-GHz
802 vertically pointing radars. IEEE Transactions on Geoscience and Remote Sensing, 54,
803 6048–6060, https://doi.org/10.1109/ TGRS.2016.2580526, 2016
804 Xu, W.: Precipitation and convective characteristics of summer deep convection over east Asia
805 observed by TRMM, Monthly Weather Review., 141, 1577-1592.
806 https://doi.org/10.1175/MWR-D-12-001

807
808 **Table 1**. Acronyms and Abbreviations Used in This Study

Acronyms and Abbreviations	Full Name
2DVD	Two-dimensional video disdrometer
A	Total two-way attenuation of 35-GHz VPR signals
ARSCL	Active remote sensing of clouds
ARM	Atmospheric Radiation Measurement
B	coefficients for cloud water attenuation
C	coefficients for rainfall attenuation
CLWP	Cloud liquid water path
D	Raindrop diameter
D_m	Mean mass-weighted raindrop diameter
D_{max}	Maximum diameters in the size distribution
D_{min}	Minimum diameters in the size distribution
DOE	Department of Energy
DSD	Drop size distribution
DVD	Doppler velocity difference
G	Two-way gaseous absorption
IWC	Ice water content
KAZR	Ka-band ARM zenith radar
LUT	Looking up table
LWP	Liquid water path
MB	Base of melting layer
MC3E	Mid-latitude continental convective clouds experiment
MMCR	Millimeter-wavelength cloud radar
MWR	Microwave radiometer
N_{DSD}	Number concentration
N_0	Intercept of ice particle size distribution
NOAA	National Oceanic and Atmospheric Administration
N_w	Scaling parameter in the drop size distribution
RLWP	Rain liquid water path
R_m	Layer-mean rain rate
RR	Rain rate

	$\mathbf{S}_{\mathbf{DSD}}^{\boldsymbol{\lambda}}$	Radar reflectivity-weighted velocity spectral density
	$\mathbf{v}_{\mathbf{DSD}}^{\boldsymbol{\lambda}}$	First reflectivity-weighted velocity spectrum moments represent the mean velocity
Vz		Raindrop terminal velocity
	$\mathbf{Z}_{\mathbf{DSD}}^{\boldsymbol{\lambda}}$	Zeroth reflectivity-weighted velocity spectrum moments represent the intrinsic (non-attenuation) reflectivity factor
$\boldsymbol{\Gamma}(\mathbf{x})$		Euler gamma function
λ		Radar wavelength
	$\boldsymbol{\sigma}_{\mathbf{b}}^{\boldsymbol{\lambda}}$	Raindrop backscattering cross section
μ		Shape parameter

Table 2. Statistics (mean differences, 95% confidence interval of mean differences, RMSEs) of D_m, RR between this study (RET) and disdrometers (2DVD, RD-80) for Case A and Case B

	Mean Differences (95% confidence interval)	RMSE
Case A: D_m (RET, 2DVD) (mm)	0.04 (-0.07, -0.01)	0.24
Case A: RR (RET, RD-80) (mm hr^{-1})	-0.45 (-0.57, -0.33)	0.96
Case A: RR (RET, 2DVD) (mm hr^{-1})	-0.61(-0.77, -0.43)	1.38
Case B: D_m (RET, 2DVD) (mm)	0.10 (-0.14, -0.07)	0.27
Case B: RR (RET, RD-80) (mm hr^{-1})	0.40 (0.19, 0.60)	1.51
Case B: RR (RET, 2DVD) (mm hr^{-1})	0.30(0.09, 0.52)	1.58

Deleted: ¶
Mean Differences¶
(95% confidence interval) ... [2]

Deleted: ¶
Mean Differences¶
(95% confidence interval) ... [1]

Table A. The brightness temperatures (TB) at 23.8 and 31.4 GHz for different assumptions of CLWP and RLWP values.

Sensitivity Test	CLWP (kg m^{-2})	RLWP (kg m^{-2})	TB at 23.8 GHz	TB at 31.4 GHz
#1	2	0	197.20	196.28
#2	1	0	186.34	177.49
#3	0	1	217.28	228.20
#4	0	2	254.51	272.09
#5	1	1	225.37	239.88

Formatted: Font: Bold

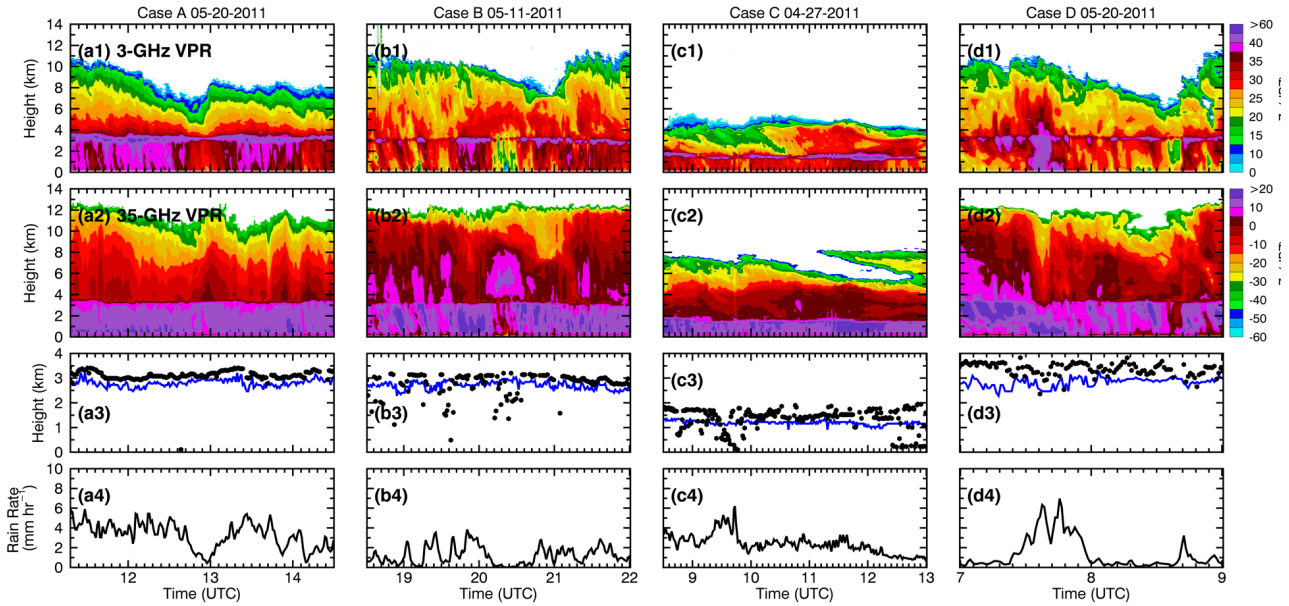

Figure 1. Time series of (a1) radar reflectivity (Z_e) from NOAA 3-GHz vertical pointing radar (VPR), (b1) radar reflectivity from ARM 35-GHz VPR, (c1) melting base (blue lines) and cloud base (black dots), and (d1) rain rates from RD-80 surface disdrometer measurement for Case A (20 May 2011, 11:20 – 14 :30 UTC); (b1)-(b4) for Case B (11 May 201, 18:30 – 22 :00 UTC); (c1)-(c4) for Case C (27 April 2011, 8:30 – 13 :00 UTC); (d1)-(d4) for Case D (20 May 2011, 7:00 – 9 :00 UTC). Note that the ranges of radar dBZ values are different in 3-GHz and 35-GHz radars.

Deleted: ¶

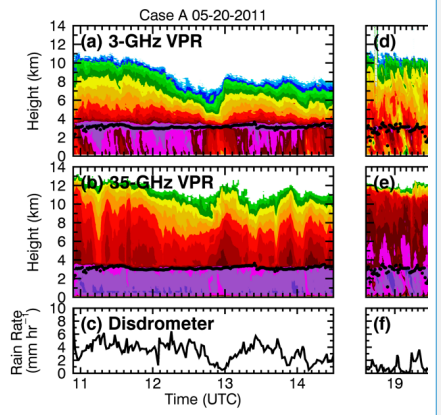

Figure 1. Time series of (a) radar reflectivity (Z_e) from NOAA 3-GHz vertical pointing radar (VPR), (b) radar reflectivity from ARM 35-GHz VPR, and (c) rain rates from RD-80 surface disdrometer measurement for Case A (20 May 2011, 11:00 – 15 :30 UTC); (d)-(f) for Case B (11 May 201, 18:30 – 23 :00 UTC); (g)-(i) for Case C (27 April 2011, 8:00 – 12 :00 UTC); (j)-(l) for Case D (20 May 2011, 7:00 – 9 :00 UTC). Ceilometer cloud base height estimates are shown with black dots at 1-minute resolution. Note that the ranges of radar dBZ values are different in 3-GHz and 35-GHz radars. ¶

Page Break

¶

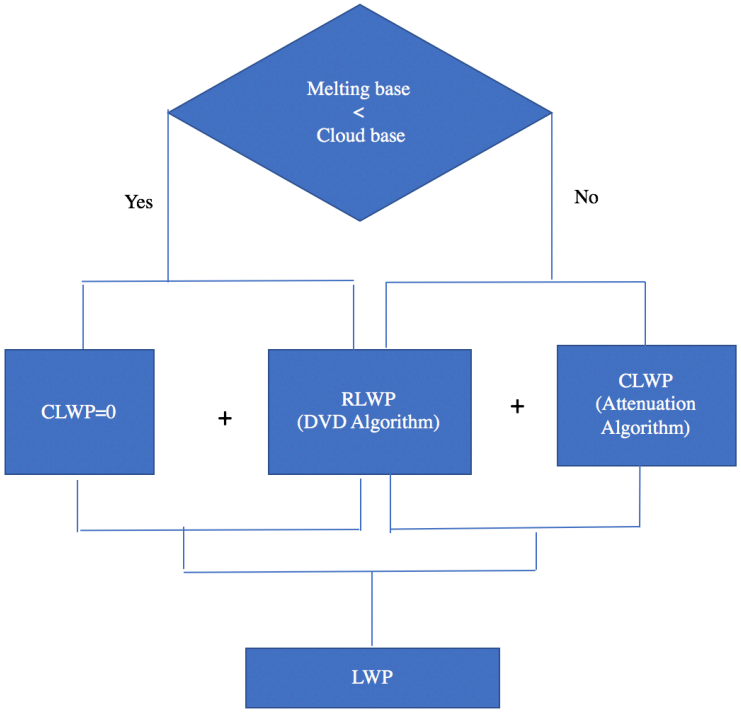

Figure 2. Algorithm flowchart to retrieve liquid water path (LWP) below melting base.

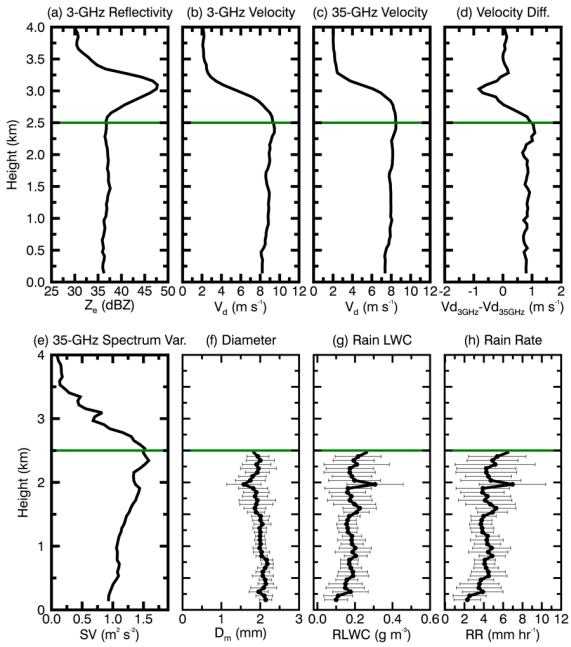

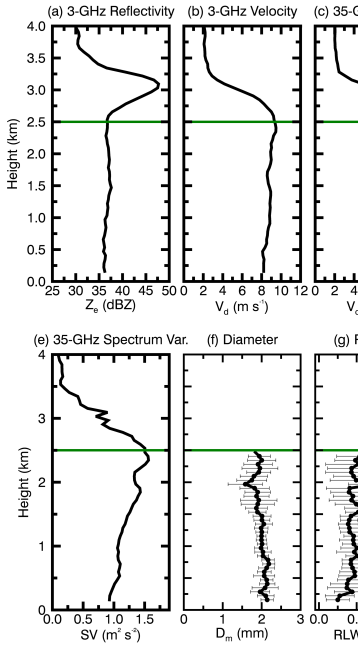

Deleted:

Figure 3. An example of illustrating the Doppler Velocity Differences (DVD) retrieval algorithm at 13:40 UTC on May 20, 2011. The inputs of the DVD retrieval algorithm are: (a) 3-GHz vertical pointing radar reflectivity factor (Z_e), (b) 3-GHz radar Doppler velocities (V_d), (c) 35-GHz radar Doppler velocities (V_d), and (e) 35-GHz radar spectrum variances (SV). The Doppler velocity difference between 3-GHz and 35 GHz is shown in (d). The outputs of the DVD retrieval algorithm are: (f) mass-weighted mean diameter D_m, (g) rain liquid water content (RLWC), and (h) rain rate (RR). Retrieval uncertainties are shown as horizontal thin black lines.

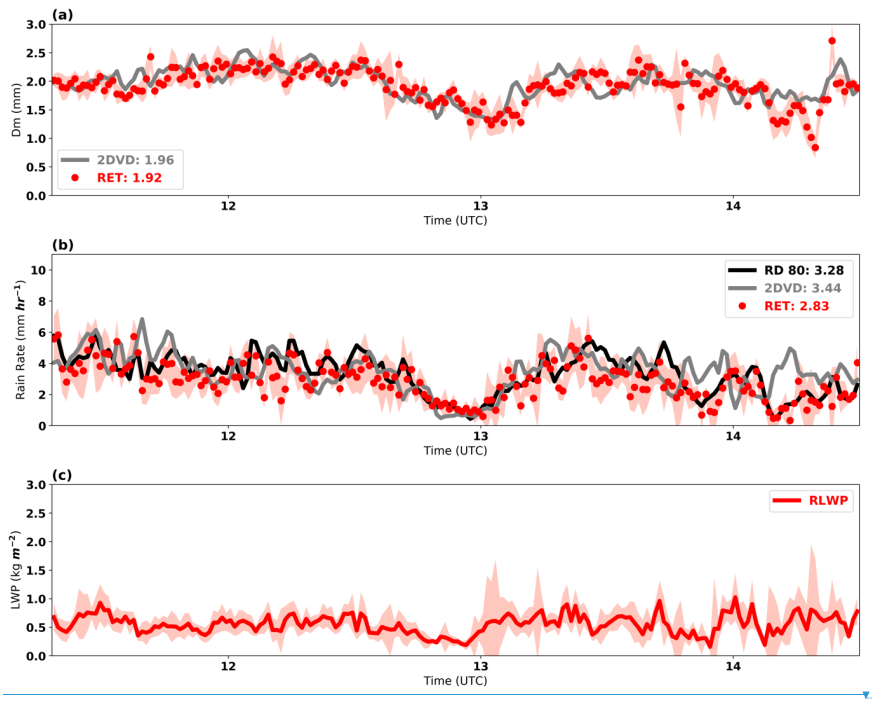

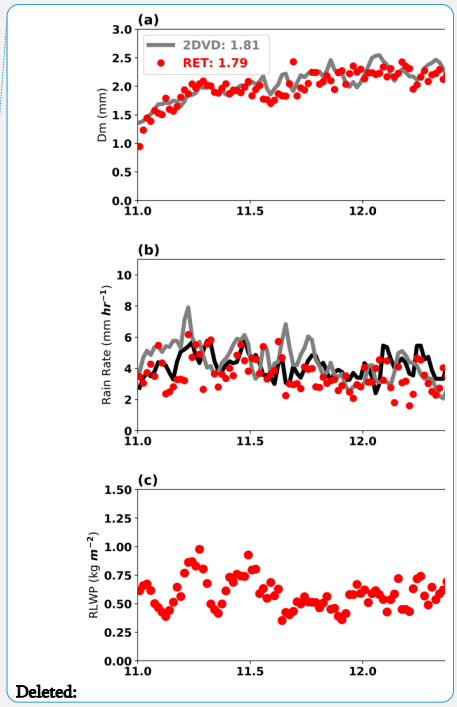

Deleted:

Figure 4. Time series of (a) retrieved (RET) (red dots) and 2DVD surface disdrometer estimated (grey line) D_m, (b) RET (red dots), 2DVD (grey line) and RD-80 (black line) surface disdrometer rain rate estimates, and (c) retrieved rain liquid water path (RLWP, red dots) for Case A (May 20, 2011. The red shading areas are the estimated retrieval uncertainties.

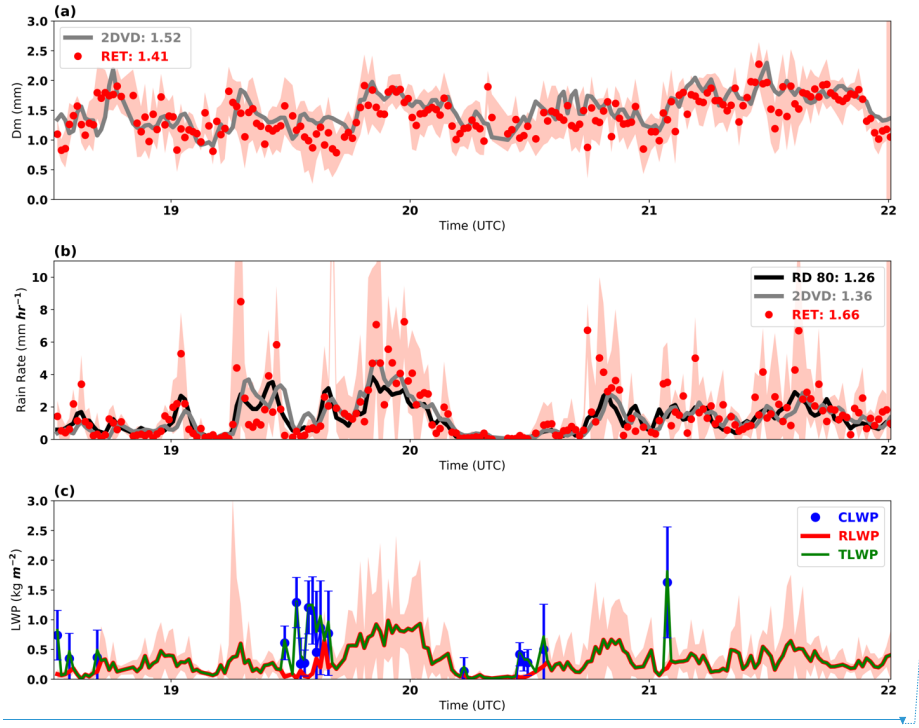

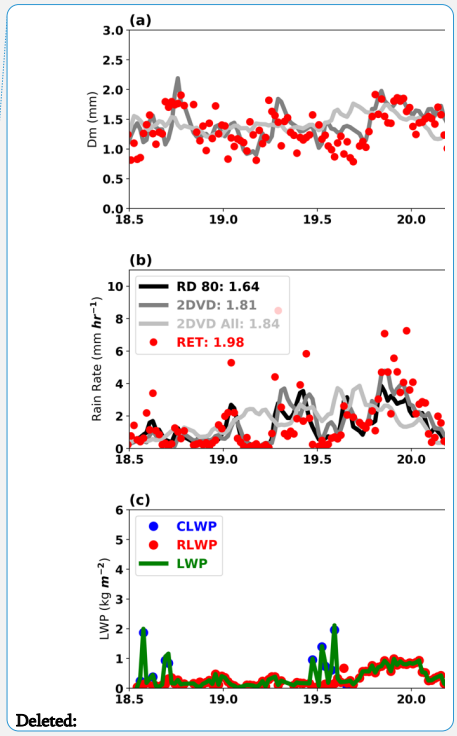

Deleted:

Figure 5. Time series of (a) retrieved (RET) (red dots) and 2DVD surface disdrometer estimated (grey lines) D_m, (b) RET (red dots), 2DVD (grey line) and RD-80 (black line) surface disdrometer rain rate estimates, and (c) rain liquid water path (RLWP, red dots), cloud liquid water path (CLWP, blue dots) and liquid water path (LWP = RLWP+CLWP, green lines) for Case B (May 11, 2011). The red shading area and blue bars are the estimated retrieval uncertainties for rain microphysical properties (D_m, rain rate and RLWP) and CLWP.

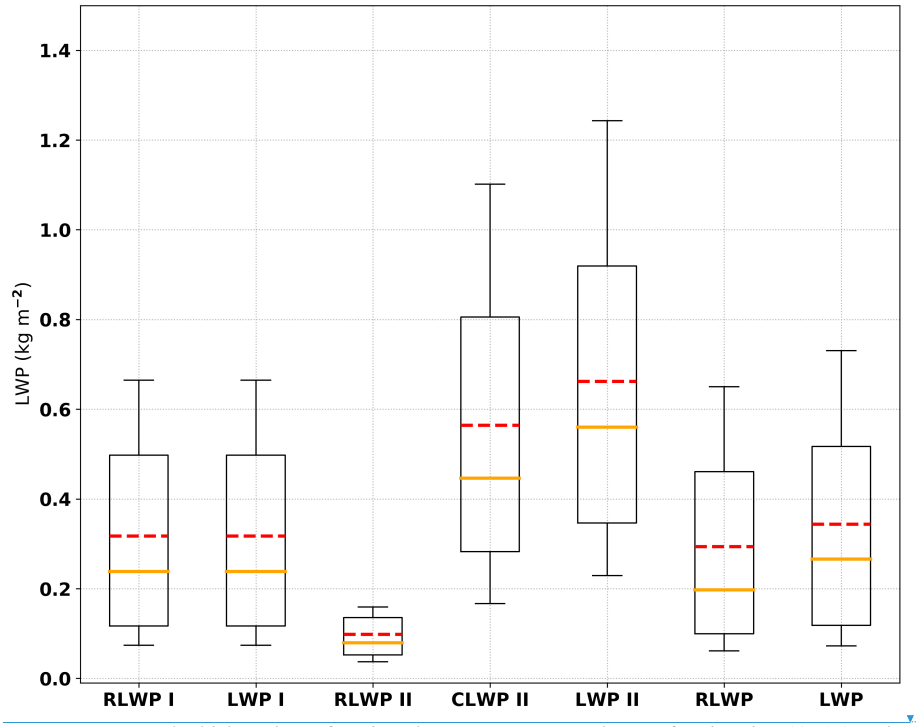

Figure 6. Box and whisker plots of retrieved RLWP, CLWP and LWP for situation (I), (II) and all samples. The horizontal orange line within the box indicates the median, boundaries of the box represent the 25th- and 75th -percentile, and the whiskers indicate the 10th- and 90th -percentile values of the results. The red dash lines represent the mean values.

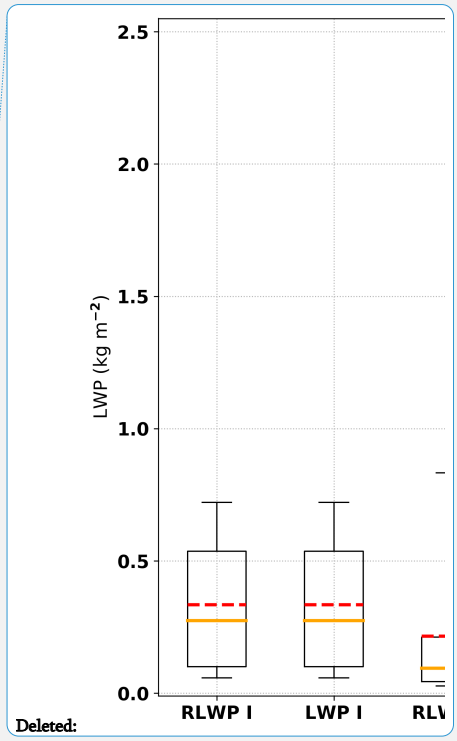

Deleted:

Deleted: indicate

Deleted: indicate

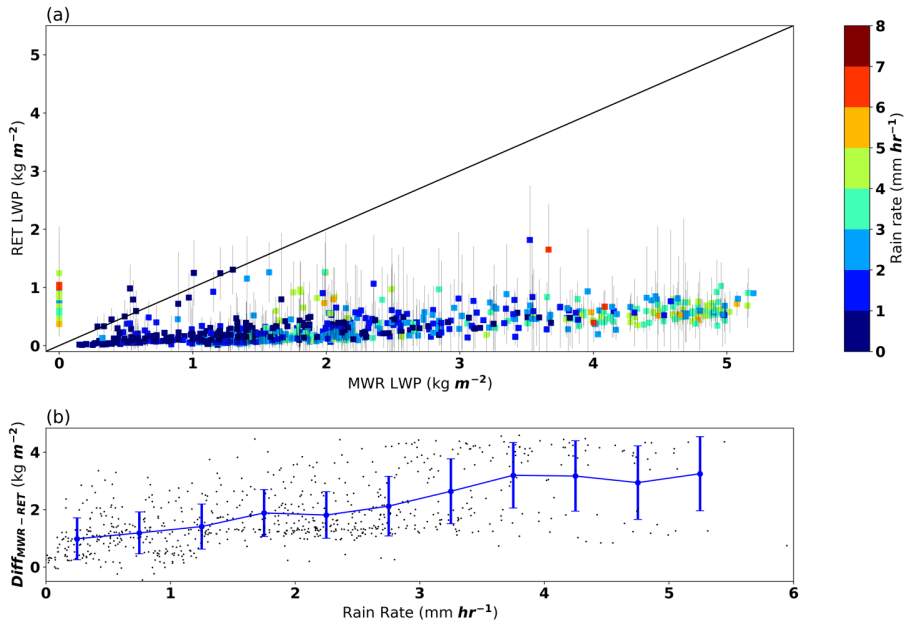

Figure 7. (a) Comparisons between LWP from microwave radiometer (MWR, in x-axis) and LWP retrievals from this study (RET, in y-axis, with estimated uncertainty in gray lines). The rain rates are indicated by colors. (b) the LWP differences between two estimations (MWR-RET), shown as a function of rain rate.

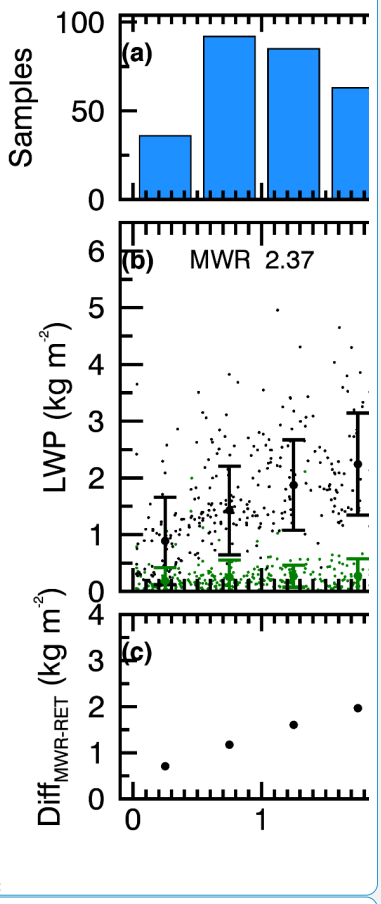

Deleted:

Deleted: Figure 7. (b) Statistic comparisons between LWP retrievals from this study (RET, dots with one standard deviation bars in green) and microwave radiometer (MWR, black dots with one standard deviation bars in black), (a) corresponding sample numbers (blue bars) in each rain rate bin (0.25 mm hr^{-1}), and (c) the LWP differences between two estimations, shown as a function of rain rate for all cases. ¶

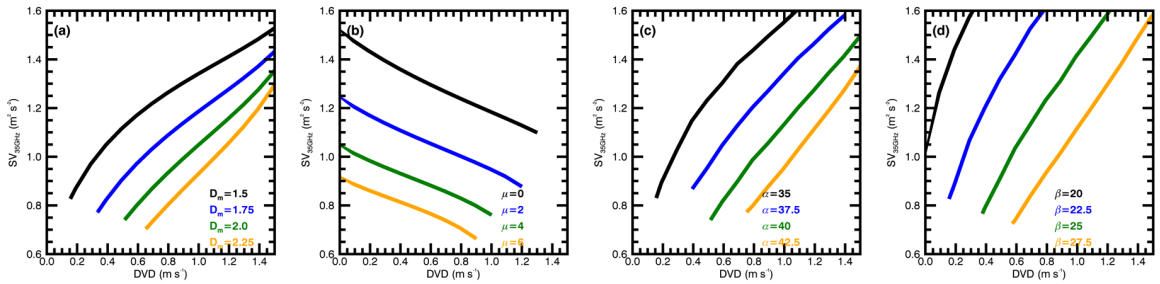

Figure A. Comparisons of (a) mass-weighted mean diameter D_m (mm), (b) shape parameter μ, (c) parameter α= 10 log(Z_{3GHz}/RLWC), and (d) parameter β = 10 log(Z_{3GHz}/RR) calculated as functions of Doppler velocity difference (DVD) and spectrum variance at 35 GHz (SV_{35GHz}). Note that the units of RLWC and RR are g m^{-3} and mm hr^{-1}.

Deleted:

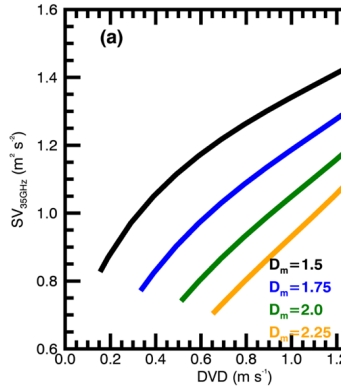

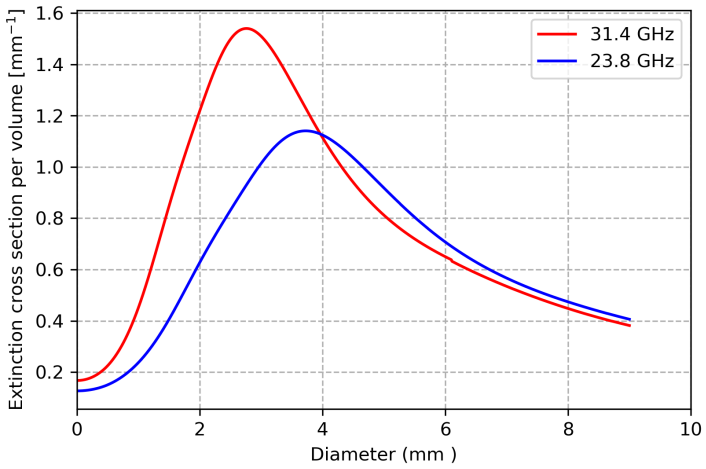

Figure B. The extinction cross section per volume as a function of the drop equivolume diameter for the two frequencies in MWR (23.8 GHz and 31.4 GHZ).

Deleted: Figure A. Comparisons of (a) mass-weighted mean diameter D_m (mm), (b) parameter $Z_{3GHz}LWC = 10 \log(Z_{3GHz}/LWC)$ (dB), and (c) parameter $Z_{3GHz}PR = 10 \log(Z_{3GHz}/RR)$ (dB) calculated as functions of Doppler velocity difference (DVD) and spectrum variance at 35 GHz (SV_{35GHz}). ¶

Formatted: Font: Bold

Formatted: Left

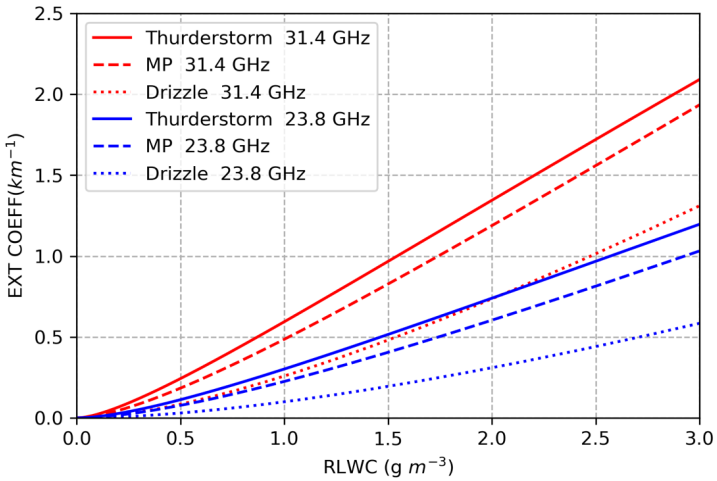

Figure C. The extinction coefficient as a function of RLWC for precipitations with three different drop size distributions (DSDs), which are for heavy precipitation (thunderstorm), moderate precipitation (MP) and drizzle precipitation (drizzle).

Formatted: Centered

Formatted: Font: Bold

Page 34: [1] Deleted	Tian, Jingjing - (jingjingtian)	4/19/19 12:47:00 AM
Page 34: [2] Deleted	Tian, Jingjing - (jingjingtian)	4/19/19 12:47:00 AM